AD-A086 401 NAVAL SURFACE WEAPONS CENTER SILVER SPRING MD F/G 20/5
INFLUENCE OF WALL IMPEDANCE ON THE ELECTRON CYCLOTRON MASER INS--ETC(U)
MAR 80 H S UHM
UNCLASSIFIED NSWC/TR-80-131 NL

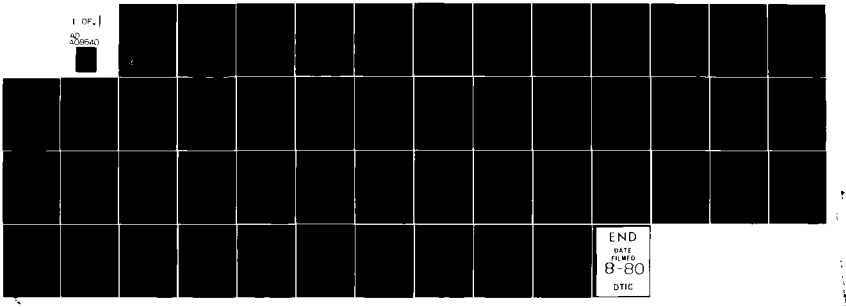

NSWC TR 80-131

INFLUENCE OF WALL IMPEDANCE ON THE ELECTRON CYCLOTRON MASER INSTABILITY

BY HAN S. UHM

RESEARCH AND TECHNOLOGY DEPARTMENT

1 MARCH 1980

Approved for public release, distribution unlimited.

NAVAL SURFACE WEAPONS CENTER

Dahlgren, Virginia 22448 • Silver Spring, Maryland 20910

UNCLASSIFIED

SECURITY CLASSIFICATION OF THIS PAGE (When Data Entered)

REPORT DOCUMENTATION PAGE	READ INSTRUCTIONS BEFORE COMPLETING FORM
1. REPORT NUMBER: NSWC TR-80-131	2. GOVT ACCESSION NO.: AD-A086401
3. RECIPIENT'S CATALOG NUMBER	
4. TITLE (and Subtitle): INFLUENCE OF WALL IMPEDANCE ON THE ELECTRON CYCLOTRON MASER INSTABILITY.	5. TYPE OF REPORT & PERIOD COVERED: Final
6. PERFORMING ORG. REPORT NUMBER	
7. AUTHOR(s): Han S. Uhm	8. CONTRACT OR GRANT NUMBER(s)
9. PERFORMING ORGANIZATION NAME AND ADDRESS: Naval Surface Weapons Center, Code R41, White Oak, Silver Spring, MD 20910	10. PROGRAM ELEMENT, PROJECT, TASK AREA & WORK UNIT NUMBERS: 61152N; ZR00001; ZR01109; R0123
11. CONTROLLING OFFICE NAME AND ADDRESS	12. REPORT DATE: 1 March 1980
	13. NUMBER OF PAGES: 49
14. MONITORING AGENCY NAME & ADDRESS (if different from Controlling Office)	15. SECURITY CLASS. (of this report): UNCLASSIFIED
	15a. DECLASSIFICATION/DOWNGRADING SCHEDULE

16. DISTRIBUTION STATEMENT (of this Report)

Approved for public release, distribution unlimited

17. DISTRIBUTION STATEMENT (of the abstract entered in Block 20, if different from Report)

18. SUPPLEMENTARY NOTES

19. KEY WORDS (Continue on reverse side if necessary and identify by block number)

Microwave Generation
Cyclotron Maser Instability
Hollow Electron Beam
Wall Impedance

20. ABSTRACT (Continue on reverse side if necessary and identify by block number)

The influence of finite wall impedance effects on the cyclotron maser instability of a hollow electron beam is investigated. The stability analysis is carried out within the framework of the linearized Vlasov-Maxwell equations, assuming that the beam thickness is much less than the radius of the beam. The formal dispersion relation for azimuthally symmetric electromagnetic perturbations is obtained, including the influence of an arbitrary value of wall impedance. One of the most important features of this analysis is that, for a purely resistive wall, the growth rate of instability is substantially reduced

DD FORM 1 JAN 73 1473 EDITION OF 1 NOV 65 IS OBSOLETE
S/N 0102-014-6601

UNCLASSIFIED

SECURITY CLASSIFICATION OF THIS PAGE (When Data Entered)

Item 20 (cont)

by allowing even a very small amount of resistivity. Moreover, the range of axial wave-numbers corresponding to instability increases rapidly as the wall resistivity is increased. Cyclotron maser stability properties in a dielectric loaded waveguide is also investigated. It is shown that by an appropriate choice of the dielectric constant ε and thickness of dielectric material, the bandwidth of instability can be increased more than twice of that for a plain conducting waveguide.

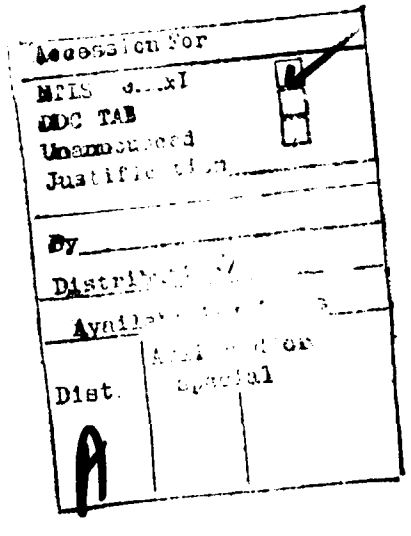

FOREWORD

The influence of finite wall impedance effects on the cyclotron maser instability of a hollow electron beam is investigated. The stability analysis is carried out within the framework of the linearized Vlasov-Maxwell equations, assuming that the beam thickness is much less than the radius of the beam. The formal dispersion relation for azimuthally symmetric electromagnetic perturbations is obtained, including the influence of an arbitrary value of wall impedance. One of the most important features of this analysis is that, for a purely resistive wall, the growth rate of instability is substantially reduced by allowing even a very small amount of resistivity. Moreover, the range of axial wave numbers corresponding to instability increases rapidly as the wall resistivity is increased. Cyclotron maser stability properties in a dielectric loaded waveguide is also investigated. It is shown that by an appropriate choice of the dielectric constant ε and thickness of dielectric material, the bandwidth of instability can be increased more than twice of that for a plain conducting waveguide.

B.F. DE SAVAGE
By direction

CONTENTS

ILLUSTRATIONS

ILLUSTRATIONS (CON'T)

I. INTRODUCTION

In recent years, there has been increasing interest in the electron cyclotron maser instability[1-9] in connection with intense microwave generation.[10-13] For the most part, previous theoretical analyses of this instability have been carried out without including the influence of finite impedance effects of a waveguide which has been previously assumed to be a perfect conductor. Although this is a reasonable assumption in the present experiments, we expect significant modification to the stability behavior when a small amount of an artificial resistivity is introduced into the waveguide wall in order for a stable operation of the microwave amplification. Moreover, to increase the bandwidth of microwave amplification, a dielectric loaded waveguide is more desirable than a pure conducting waveguide. However, in the dielectric loaded waveguide, the impedance of wall is purely reactive. In this paper, we investigate the influence of finite wall impedance effects on the cyclotron maser instability of a hollow electron beam in a waveguide with an arbitrary impedance Z.

Equilibrium and stability properties are calculated for the specific choice of electron distribution function [Eq. (3)].

$$f_e^o(H,P_\theta,P_z)=(\omega_c N_e/4\pi^2 mc^2)\delta(\gamma-\hat{\gamma})\delta(p_z-\hat{p})\delta(P_\theta-P_o) \quad ,$$

where $H=\gamma mc^2$ is the energy, P_θ is the canonical angular momentum, P_z is the axial momentum, $\omega_c=eB_o/\hat{\gamma}mc$ is the electron cyclotron frequency, and N_e is the number of electrons per unit axial length. The stability analysis in this paper is carried out within the framework of the linearized Vlasov-Maxwell equations, assuming that the beam thickness is much less than the equilibrium radius R_o of the beam and that $\nu/\hat{\gamma}<<1$, where ν is Budker's parameter.

The formal stability analysis for azimuthally symmetric electromagnetic perturbations ($\partial/\partial\theta=0$) is carried out in Sec. II, including the important influence of finite wall impedance Z, which in general is an arbitrary function of the eigenfrequency ω and axial wavenumber k. The dispersion relation of cyclotron maser instability in Eq. (20), when combined with Eqs. (17) and (18), constitutes one of the main results of this paper and can be used to investigate stability properties for a broad range of system parameters. In this regard, we emphasize that Eq. (20) is derived with *no a priori* assumption that the electron beam is tenuous, or that the impedance of wall is independent of ω and k.

In Sec. III, sum of magnetic wave admittances $b_- + b_+$ in Eq. (20) can be significantly simplified by making use of tenuous beam limit ($\nu/\hat{\gamma}\to 0$). In the absence of a beam, the vacuum transverse electric (TE) mode dispersion relation is given by Eq. (26)

$$(\omega^2/c^2-k^2)R_w^2=x_{on}^2(\omega,k) \ ,$$

where c is the speed of light in vacuo, R_w is the radius of impedance wall, x_{on} is the nth root of $Z=J_1(x_{on})/x_{on}J_o(x_{on})$, and $J_\ell(x)$ is the Bessel function of the first kind of order ℓ. The root x_{on} is calculated numerically for a given complex value of wall impedance Z. The detailed dependence of the root x_{on} in Eq. (26) on the eigenfrequency ω and axial wavenumber k is particularly important in connection with the gain and bandwidth of a microwave amplification by the cyclotron maser instability.

In Sec. IV, a detailed analytic and numerical investigation of the cyclotron maser instability is carried out for a wall impedance independent of the eigenfrequency ω and axial wavenumber k (i.e., $\partial Z/\partial\omega=0$, $\partial Z/\partial k=0$). Defining the wall impedance Z by $Z=|Z|\exp(-i\phi)$, stability properties of cyclotron maser instability are investigated for a broad range

of the magnitude $|Z|$ and the phase angle ϕ. One of the most important features of this analysis is that, for a purely resistive wall characterized by $\phi=90°$, the growth rate is substantially reduced by introducing even a very small amount of resistivity into the wall. This feature represents a general tendency for all radial mode number n. Moreover, the range of the normalized axial wavenumber kc/ω_c corresponding to instability increases rapidly as the resistivity of wall is increased.

Cyclotron maser stability properties in a dielectric loaded waveguide are investigated in Sec. V, assuming that the impedance of dielectric material is purely reactive. It is shown that stability properties of cyclotron maser instability exhibit a sensitive dependence on the dielectric constant ε and thickness of dielectric material. By an appropriate choice of ε and thickness of dielectric material, the bandwidth of instability can be increased more than twice of that for a plain conducting waveguide. Moreover, dielectric material reduces the radial wavelength of the waveguide mode, thereby significantly modifying the nature of perturbations. The influence of self-dielectric effects of an electron beam itself on the stability behavior is investigated. However, for a low density beam (i.e., $\nu/\hat{\gamma}<<0.005$) with small transverse velocity, self-dielectric effects are insignificant.

II. LINEARIZED VLASOV-MAXWELL EQUATIONS

The equilibrium configuration consists of a hollow relativistic electron beam propagating parallel to a strong, externally applied magnetic field $B_0\hat{e}_z$. The radius of the electron beam is denoted by R_o, and a finite impedance wall is located at radius $r=R_w$. Cylindrical polar coordinates (r,θ,z) are introduced. In the present analysis, we assume that

$$\nu/\hat{\gamma} \ll 1 \ , \tag{1}$$

where $\nu=N_e e^2/mc^2$ is Budker's parameter,

$$N_e=2\pi\int_o^{R_c} dr\, r\, n_e^o(r) \ , \tag{2}$$

is the number of electrons per unit axial length, $n_e^o(r)$ is the equilibrium electron density, c is the speed of light in vacuo, -e and m are the electron charge and rest mass, respectively, and $\hat{\gamma}mc^2$ is the characteristic electron energy in the laboratory frame. Consistent with the low-intensity assumption in Eq. (1), we also neglect the influence of equilibrium self-field.

In the present article, we investigate the stability properties associated with the beam distribution function

$$f_e^o(H,P_\theta,P_z)= \frac{\hat{\omega}_c N_e}{4\pi^2\hat{\gamma}mc^2}\,\delta(\gamma-\hat{\gamma})\,\delta(p_z-\hat{p})\,\delta(P_\theta-P_o) \ , \tag{3}$$

where $H=\gamma mc^2=(m^2c^4+c^2p^2)^{1/2}$ is the total energy, $P_z=p_z$ is the axial canonical momentum, $P_\theta=r[P_\theta-(e/2c)rB_o]$ is the canonical angular momentum, $\hat{\omega}_c = eB_o/mc$ is the nonrelativistic electron cyclotron frequency,

$$P_o= -(e/2c)(R_o^2-r_L^2)B_o \ , \tag{4}$$

is the canonical angular momentum of an electron with Larmor radius,

$$r_L=[(\gamma^2-1)c^2/\hat{\omega}_c^2-(\hat{p}/m\hat{\omega}_c)^2]^{1/2} \ , \tag{5}$$

and p is a constant. For a notational convenience in the subsequent analysis, we also introduce the definitions $\beta_z=\hat{p}/\hat{\gamma}mc$ and $\beta_\perp=(1-\beta_z^2-1/\hat{\gamma}^2)^{1/2}$. The equilibrium properties of an electron beam described by Eq. (3) can be found in the previous literatures.[5,7]

In the subsequent stability analysis, we make use of the linearized Vlasov-Maxwell equations of azimuthally symmetric perturbations ($\partial/\partial\theta=0$) about a tenuous, hollow beam equilibrium described by Eq. (3). We adopt a normal-mode approach in which all perturbations are assumed to vary with time and z according to

$$\delta\psi(\underset{\sim}{x},t)=\hat{\psi}(r)\exp[i(kz-\omega t)] \ ,$$

where $Im\omega>0$ Here, ω is the complex eigenfrequency and k is the axial wavenumber. The Maxwell equations for the perturbed electric and magnetic field amplitudes can be expressed as

$$\nabla \times \hat{\underset{\sim}{E}}(\underset{\sim}{x})=i(\omega/c)\hat{\underset{\sim}{B}}(\underset{\sim}{x}) \ ,$$

$$\nabla \times (1/\mu)\hat{\underset{\sim}{B}}(\underset{\sim}{x})=(4\pi/c)\hat{\underset{\sim}{J}}(\underset{\sim}{x})-i(\omega/c)\varepsilon\,\hat{\underset{\sim}{E}}(\underset{\sim}{x}) \ , \qquad (6)$$

where ε and μ are the dielectric constant and permeability, respectively, of the background material, $\hat{\underset{\sim}{E}}(\underset{\sim}{x})$ and $\hat{\underset{\sim}{B}}(\underset{\sim}{x})$ are the perturbed electric and magnetic fields, respectively, and

$$\hat{\underset{\sim}{J}}(\underset{\sim}{x})= -e\int d^3p\ \underset{\sim}{v}\ \hat{f}_e(\underset{\sim}{x},\underset{\sim}{p}) \qquad (7)$$

is the perturbed current density. Note that $\varepsilon=\mu=1$ in vacuo. In Eq. (7),

$$\hat{f}_e(\underset{\sim}{x},\underset{\sim}{p})=e\int_{-\infty}^{o}d\tau\ \exp(-i\omega\tau)\left[\hat{\underset{\sim}{E}}(\underset{\sim}{x}')+\frac{\underset{\sim}{v}'\times\hat{\underset{\sim}{B}}(\underset{\sim}{x}')}{c}\right]\frac{\partial}{\partial\underset{\sim}{p}'}f_e^o \qquad (8)$$

is the perturbed distribution function, $\tau=t'-t$, and the particle trajectories $\underset{\sim}{x}'(t')$ and $\underset{\sim}{p}'(t')$ satisfy $d\underset{\sim}{x}'/dt'=\underset{\sim}{v}'$ and $d\underset{\sim}{p}'/dt'=-e\underset{\sim}{v}'\times B_o\,\hat{\underset{\sim}{e}}_z/c$, with "initial" conditions $\underset{\sim}{x}'(t'=t)=\underset{\sim}{x}$ and $\underset{\sim}{v}'(t'=t)=\underset{\sim}{v}$.

Making use of Eq. (6), it is straightforward to show that

$$\hat{B}_r(r) = -(kc/\omega)\hat{E}_\theta(r) \ ,$$

$$\hat{B}_z(r) = -i(c/\omega r)[\partial(r\hat{E}_\theta)/\partial r] \ , \tag{9}$$

and

$$\mu \frac{\partial}{\partial r}\left[\frac{1}{\mu r}\frac{\partial}{\partial r}(r\hat{E}_\theta)\right] + p^2\hat{E}_\theta = -\frac{4\pi i\omega\mu}{c}\hat{J}_\theta \tag{10}$$

where

$$p^2 = \omega^2\mu\varepsilon/c^2 - k^2 \ , \tag{11}$$

$\hat{E}_\theta$ is the azimuthal component of perturbed electric field, and $\hat{B}_r$ and $\hat{B}_z$ are the radial and axial components, respectively, of the perturbed magnetic field. The field equations (9) and (10) represent the transverse electric (TE) waveguide modes. For the cyclotron maser instability, it is well established[1,9] that the beam cyclotron resonance mode couples much more strongly with the TE waveguide mode than the transverse magnetic (TM) waveguide mode. In this regard, the present analysis is restricted to the TE waveguide mode.

The perturbed azimuthal electric field $\hat{E}_\theta(r)$ is continuous across the beam inner and outer boundaries $r=R_1$ and $r=R_2$. Integrating Eq. (10) from $r=R_1-\delta$ to $r=R_2+\delta$ and taking the limit $\delta\to 0_+$, we obtain the approximate result[1]

$$\hat{B}_z(R_2^+) - \hat{B}_z(R_1^-) = -\frac{4\pi}{c}\int_{R_1^-}^{R_2^+} dr\hat{J}_\theta(r) \ , \tag{12}$$

where $\psi(R_2^\pm)$ denotes $\lim_{\delta\to 0_+}\psi(R_2\pm\delta)$, and use has been made of the hollow beam approximation (Thickness of the beam is much less than the beam radius R_o). For convenience in the subsequent analysis, we introduce the normalized magnetic wave admittance[1] $b_\pm$ defined at the inner and outer surfaces of the electron beam by

$$b_- = -i\omega/p_1^2 cR_o)\hat{B}_z(R_1^-)/\hat{E}_\theta(R_o) \ ,$$
$$b_+ = i(\omega/p_1^2 cR_o)\hat{B}_z(R_2^+)/\hat{E}_\theta(R_o) \ , \tag{13}$$

where

$$p_1^2 = \omega^2/c^2 - k^2 \ . \tag{14}$$

Moreover, we also define the wave impedance $Z(\omega,k)$ of the wall as

$$Z(\omega,k) = -i(c/\omega R_w)\hat{E}_\theta(R_w)/\hat{B}_z(R_w) \ , \tag{15}$$

where R_w is the radius of an impedance wall.

Since the perturbed current density vanishes in the vacuum region outside the beam, it is obvious that the solution to Eq. (10) in the vacuum region is given by

$$\hat{E}_\theta(r) = \begin{cases} A\ J_1(p_1 r), & r<R_1 \ , \\ B\ J_1(p_1 r)+C\ N_1(p_1 r), & R_2<r<R_w, \end{cases} \tag{16}$$

where $J_\ell(p_1 r)$ and $N_\ell(p_1 r)$ are Bessel functions of the first and second kind, respectively, of order ℓ. Making use of Eqs. (15) and (16), and the thin beam approximation ($R_1 \simeq R_2 \simeq R_o$), we express the sum b_-+b_+ of the wave admittance in Eq. (13) as

$$b_-+b_+ = \frac{[2g(\xi)/\pi](R_w/R_o\xi)^2}{J_1(\xi R_o/R_w)[J_1(\xi R_o/R_w)+g(\xi)N_1(\xi R_o/R_w)]} \ , \tag{17}$$

where $\xi = p_1 R_w$, and

$$g(\xi) = \frac{\xi J_o(\xi)}{N_1(\xi)-\xi Z N_o(\xi)} \left[Z - \frac{J_1(\xi)}{\xi J_o(\xi)}\right]. \tag{18}$$

Substituting Eq. (13) into Eq. (12), we obtain

$$(b_-+b_+) = -i\ \frac{4\pi\omega R_w^2}{c^2\xi^2 R_o \hat{E}_\theta(R_o)}\ dr\ \hat{J}_\theta(r) \tag{19}$$

After some tedious but straightforward algebraic manipulation with Eqs. (7), (8) and (9), we obtain the dispersion relation of the cyclotron maser instability

$$b_- + b_+ = - \frac{\nu \beta_\perp^2}{2\hat{\gamma}\xi^2} \left(\frac{R_w}{R_o} \right)^2 \frac{\omega^2 - k^2 c^2}{(\omega - k\beta_z c - \omega_c)^2} , \tag{20}$$

where $\omega_c = \omega_c / \hat{\gamma}$ is the electron cyclotron frequency on the laboratory frame, and use has been made of the assumption $\beta_\perp^2 << 1$. For a detailed derivation of Eq. (20), we urge the reader to review the previous literatures.[1,3,5] In the remainder of this article, we investigate the stability properties of Eq. (20) for various wall impedance Z on Eq. (18).

III. LIMIT OF A TENUOUS BEAM

To simplify the expressions for the sum b_-+b_+ of the wave admittance in Eq. (17), it is useful to consider the limit where the beam density is very tenuous, i.e.,

$$\nu/\dot{\gamma} \to 0 \tag{21}$$

In this absence of a beam, the vacuum TE mode dispersion relation is given by

$$Z=J_1(\xi)/\xi J_o(\xi) \ , \tag{22}$$

where $Z(\omega,k)$ is the wave impedance of the wall [Eq. (15)] and $\xi=(\omega^2/c^2-k^2)^{1/2}R_w$. Substituting Eq. (22) into Eq. (18), we can simplify Eq. (17) by

$$b_-+b_+ = -\left[\frac{R_w J_o(\xi)}{R_o J_1(\xi R_o/R_w)}\right]^2 \left[Z-\frac{J_1(\xi)}{\xi J_o(\xi)}\right] \tag{23}$$

For a convenience in future analysis, we define the nth root of Eq. (22) by

$$\xi=x_{on}(\omega,k)=x_r(\omega,k)-i\ x_i(\omega,k) \tag{24}$$

for a specified wall impedance

$$Z=|Z|\exp(-i\phi)=Z_r+iZ_i \ . \tag{25}$$

For a very tenuous beam [Eq. (21)], it is evident from Eqs. (22) and (24) that

$$(\omega^2/c^2-k^2)R_w^2=x_{on}^2(\omega,k) \tag{26}$$

is a good approximation to the dispersion relation in Eq. (20). The right-hand side of Eq. (20) describes the beam-produced modifications to the vacuum dispersion relation (26). We remind the reader that the nth root x_{on} is a function of the eigenfrequency ω and axial wavenumber

k in general. For an impedance with a small magnitude satisfying $|Z|<<1$, we obtain

$$x_{on}=\alpha_{on}[1+|Z|\exp(-i\phi)] \tag{27}$$

from Eqs. (22) and (25). Therefore, the vacuum waveguide mode for zero wall impedance can be expressed as

$$(\omega^2/c^2-k^2)R_w^2=\alpha_{on}^2 \tag{28}$$

where α_{on} is the nth root of $J_1(\alpha_{on})=0$, which is independent of ω and k.

Figure 1 is the contours of constant phase angle ϕ and magnitude $|Z|$ of the function $Z=J_1(x_{on})/x_{on}J_o(x_{on})$ in the plane of the root $x_{on}=x_r-ix_i$ for (a) n=1 and (b) n=2. We note from Fig. 1 that the nth root x_{on} of Eq. (22) approaches to α_{on} and the magnitude of wall impedance is reduced to zero. On the other hand, the nth root x_{on} approaches to β_{on} by increasing the magnitude $|Z|$ to infinity. Here β_{on} is the nth root of $J_o(\beta_{on})=0$. We also emphasize that for specified values of $|Z|$ and ϕ, the root $x_{on}=x_r-ix_i$ is determined from Fig. 1. For example, for $|Z|=0.3$, $\phi=90°$ and n=1, we find from Fig. 1 that $x_r=3.12$ and $x_i=0.82$. Obviously, the root x_{on} of Eq. (22) is a very complicated function of the wall impedance Z.

The dependence of the nth root x_{on} on the eigenfrequency ω and axial wavenumber k is particularly important in connection with the gain and bandwidth of a microwave amplification by the cyclotron maser instability. Shown in Fig. 2 are schematic drawings of the curve $\omega=(k^2c^2+\alpha_{on}^2c^2/R_w^2)^{1/2}$ corresponding to zero wall impedance and the curve $\omega=(k^2c^2+x_{on}^2c^2/R_w^2)^{1/2}$ corresponding to an arbitrary wall impedance. The straightline $\omega=k\beta_z c+\omega_c$ is the cyclotron resonance mode. It is important to note from Fig. 2 that the interaction region of cyclotron resonance mode with vacuum waveguide dispersion relation is increased substantially by an appropriate

choice of the wall impedance (x_{on}). In this regard, we conclude that the growth rate or the bandwidth of cyclotron maser instability can be considerably improved when the functional dependence of the wall impedance on ω and k is matched with the cyclotron resonance mode in a broad range of k space. However, a detail investigation of wall impedance is required. Previous studies[14] indicate that a proper waveguide structure provides a necessary wall impedance. The influence of nonuniform wall impedance on cyclotron maser instability is currently under investigation by authors for a broad range of physical parameters and waveguide structures. As a simple example, we present, in Sec. V, the cyclotron maser instability in a dielectric loaded waveguide.

IV. CYCLOTRON MASER INSTABILITY IN A WAVEGUIDE WITH CONSTANT WALL IMPEDANCE

The cyclotron maser stability properties of a hollow electron beam in a vacuum waveguide with general impedance are investigated in this section, assuming that impedances of the wall are independent of the eigenfrequency ω and the axial wavenumber k, i.e.,

$$\partial Z/\partial\omega=0, \quad \partial Z/\partial k=0 \tag{29}$$

Taylor expanding Eq. (23) about $(\omega^2/c^2-k^2)R_w^2=x_{on}^2$ with Eq. (29), it is straightforward to show that b_-+b_+ can be approximated in leading order by

$$b_-+b_+= \frac{R_w^2}{2x_{on}^2}\left(\frac{R_w}{R_o}\right)^2 \frac{J_1^2(x_{on})-J_o(x_{on})J_2(x_{on})}{J_1^2(x_{on}R_o/R_w)}\left(\frac{\omega^2}{c^2}-k^2-\frac{x_{on}^2}{R_w^2}\right). \tag{30}$$

Substituting Eq. (30) into Eq. (20) and making use of Eq. (24), we obtain the approximate dispersion relation

$$\frac{\omega^2}{c^2}-k^2-\frac{x_{on}^2}{R_w^2} = -\frac{\nu\beta_\perp^2}{\hat{\gamma}R_w^2}\frac{J_1^2(x_{on}R_o/R_w)}{J_1^2(x_{on})-J_o(x_{on})J_2(x_{on})}\frac{\omega^2-k^2c^2}{(\omega-k\beta_z c-\omega_c)^2}, \tag{31}$$

for a tenuous thin beam. Stability analysis of the dispersion relation in Eq. (31) is carried out in the remainder of this section for a broad range of physical parameters.

In order to investigate the influence of wall resistivity on stability behavior, the analysis of the dispersion relation in Eq. (31) is carried out for a wall impedance with a small magnitude satisfying $|Z|\ll 1$. In this limit, we choose the wall radius R_w according to

$$R_w=\alpha_{on}c/\omega_c\gamma_z \tag{32}$$

for the present purposes. Here γ_z is defined by $\gamma_z^2=(1-\beta_z^2)^{-1}$. Equation (32) ensures that the group velocity of the vacuum waveguide mode for

$|Z|=0$ is equal to the beam velocity for a certain k value.[3] Making use of Eq. (32) and defining the normalized Doppler-shifted eigenfrequency

$$\chi=(\omega-k\beta_z c-\omega_c)/\omega_c \ , \tag{33}$$

it is straightforward to show that the dispersion relation in Eq. (31) can be expressed as

$$\chi^4+2\left(\frac{k\beta_z c}{\omega_c}+1\right)\chi^3+\left[\left(\frac{k\beta_z c}{\omega_c}+1\right)^2-\left(\frac{kc}{\omega_c}\right)^2-\left(\gamma_z\frac{x_{on}}{\alpha_{on}}\right)^2\right]\chi^2$$

$$+\frac{\nu}{\hat{\gamma}}\left(\gamma_z^2\beta_\perp\frac{x_{on}}{\alpha_{on}^2}\right)^2\frac{J_1^2(x_{on}R_o/R_w)}{J_1^2(x_{on})-J_o(x_{on})J_2(x_{on})}=0 \ . \tag{34}$$

The normalized growth rate $\chi_i=\mathrm{Im}\chi$ and Doppler-shifted real frequency $\chi_r=\mathrm{Re}\chi$ have been calculated numerically from Eq. (34) for $\nu=0.002$, $\hat{\gamma}=1.118$, $\beta_\perp=0.4$ and several different values of wall impedance Z. For specified values of Z, the root x_{on} is determined from Fig. 1. For example, we find from Fig. 1 that $x_{on}=(x_r,x_i)=(3.82, 0.167)$ for $Z=(|Z|, \phi)=(0.045, 90°)$.

Although the present experiments of the cyclotron maser instability are carried out in a lossless cylindrical conductor, it is necessary to investigate the stability properties for a resistive waveguide, since an artificial resistivity of the wall is sometimes required for a stable operation of the microwave amplification. In this regard, we investigate the dispersion relation in Eq. (34) for a pure resistive wall characterized by $\phi=90°$. Shown in Fig. 3 are plots of (a) the normalized growth rate χ_i and (b) the normalized Doppler-shifted real frequency χ_r versus kc/ω_c obtained from Eq. (34) for n=1, $R_o/R_w=0.5$, $\phi=90°$, and several values of $|Z|$. In Fig. 3(b), χ_r is plotted only for the ranges of kc/ω_c corresponding to instability ($\chi_i>0$). Several features are noteworthy from Fig. 3. First, the maximum growth rate decreases as the magnitude $|Z|$ of wall

impedance is increased. The growth rate is substantially reduced by introducing even a very small amount of resistivity into the wall. As evident from Eq. (34) and Fig. 1, this feature represents a general tendency for all radial mode numbers n. Second, the range of kc/ω_c corresponding to instability increases rapidly as the resistivity of the wall is increased. This mechanism somehow broadens the bandwidth of microwave amplification. Third, for lossless conductor, the Doppler-shifted real frequency increases abruptly when the wavenumber k approaches to the k-space boundary corresponding to marginal stability ($\chi_i=0$). However, resistivity of the wall levels the Doppler-shifted real frequency [Fig. 3(b)].

The dependence of stability properties on phase angle ϕ of the impedance is illustrated in Fig. 4 where the normalized growth rate χ_i is plotted versus kc/ω_c for n=1, $R_o/R_w=0.5$, $|Z|=0.05$ and several different phase angles ϕ. Since the plot of the Doppler-shifted real frequency has a form similar to that of Fig. 3(b), it is not shown in Fig. 4. Evidently from Fig. 4, the maximum growth rate occurs at the phase angle $\phi=180°$. For this particular magnitude of impedance ($|Z|=0.05$), the growth rate of instability is reduced sharply as the phase angle of impedance is reduced to zero.

To investigate the cyclotron maser instability for a purely reactive impedance[15] characterized by $\phi=0°$ or $\phi=180°$, we analyze the dispersion relation in Eq. (31) for different values of x_{on} with $x_i=0$. In order to maximize the growth rate and efficiency of microwave amplification we choose[3]

$$R_w=x_{on}c/\omega_c\gamma_z,\quad R_o/R_w=\alpha_{11}/x_{on}\ , \tag{35}$$

where α_{11} is the first root of $J_1'(\alpha_{11})=0$ and $J_1'(x)=dJ_1/dx$. Making use of Eqs. (33) and (35), we can show that the dispersion relation in

Eq. (31) is expressed as

$$\chi^4+2\left(\frac{k\beta_z c}{\omega_c}+1\right)\chi^3+\left[\left(\frac{k\beta_z c}{\omega_c}+1\right)^2-\left(\frac{kc}{\omega_c}\right)^2-\gamma_z^2\right]\chi^2$$

$$+\frac{\nu}{\hat{\gamma}}\left(\frac{\gamma_z^2\beta_\perp}{x_{on}}\right)^2\frac{J_1^2(\mu_{11})}{J_1^2(x_{on})-J_o(x_{on})J_2(x_{on})}=0\ . \qquad (36)$$

Figure 5 presents plots of the normalized maximum growth rate (solid line) and R_o/R_w (broken line) versus $x_{on}=x_r$ obtained from Eqs. (36) and (35), respectively, for $\nu=0.002$, $\hat{\gamma}=1.118$, and $\beta_\perp=0.4$. Numerical calculation indicates that the maximum growth rate occurs at the wavenumber $k\approx 0.15\omega_c/c$ for the range $2\leq x_{on}\leq 4$ as shown in Fig. 5. We note from Fig. 5 that the growth rate of instability is substantially increased by reducing the value x_{on} to two. Moreover, it may be possible that further increase of the growth rate can be attainable by reducing the value x_{on} less than two and by arranging suitably the beam radius so that electrons never hit the wall [see Eqs. (31) and (36)].

V. CYCLOTRON MASER INSTABILITY IN A DIELECTRIC LOADED WAVEGUIDE

In this section, we investigate the cyclotron maser stability properties of a hollow electron beam in a dielectric loaded waveguide. As illustrated in Fig. 6, a hollow electron beam with radius R_o is propagating through a cylindrical dielectric material with its inner radius R_w. A grounded cylindrical conducting wall is located at radius R_c. In general, the permeability μ of a dielectric material differs from unity by only a few parts in 10^5 ($\mu>1$ for paramagnetic substances, $\mu<1$ for diamagnetic substances). Therefore, we make the approximation $\mu=1$ in the calculation in this section. In this regard, the perturbed azimuthal electric field $\hat{E}_\theta(r)$ and axial magnetic field $\hat{B}_z(r)$ are continuous across the dielectric boundary $r=R_w$. From Eq. (10), we obtain

$$\frac{\partial}{\partial r}\left[\frac{1}{r}\frac{\partial}{\partial r}\left(r\hat{E}_\theta\right)\right]+p_2^2\hat{E}_\theta=0 \quad , \tag{37}$$

inside the dielectric material. Here the parameter p_2 is defined by

$$p_2^2=\omega^2\varepsilon/c^2-k^2 \quad . \tag{38}$$

The solution to Eq. (37) can be expressed as

$$\hat{E}_\theta(r)=A[J_1(p_2r)-J_1(\zeta)N_1(p_2r)/N_1(\zeta)] \quad , \tag{39}$$

where A is an arbitrary constant and $\zeta=R_cp_2=R_c(\omega^2\varepsilon/c^2-k^2)^{1/2}$. Obviously Eq. (39) satisfies the boundary condition $\hat{E}_\theta(r=R_c)=0$. Substituting Eq. (39) into Eq. (9) and making use of the boundary conditions at $r=R_w$, we obtain the wave impedance $Z(\omega,k)$

$$Z(\omega,k)=\frac{J_1(\eta)N_1(\zeta)-J_1(\zeta)N_1(\eta)}{\eta[J_o(\eta)N_1(\zeta)-J_1(\zeta)N_o(\eta)]} \quad , \tag{40}$$

from the definition in Eq. (15). In Eq. (40), the parameter η is defined by $\eta=R_wp_2=R_w(\omega^2\varepsilon/c^2-k^2)^{1/2}$. Note from Eq. (40) that the wall impedance of dielectric loaded waveguide is a function of eigenfrequency ω and

axial wavenumber k. Since the dielectric constant ε is always greater than unity, we note from Eqs. (14) and (38) that $p_2 > p_1$. We therefore conclude from the definitions $\xi=p_1R_w$, $\eta=p_2R_w$ and $\zeta=p_2R_c$ that

$$R_w/R_c=\eta/\zeta \tag{41}$$

and

$$\xi\leq\eta\leq\zeta \ . \tag{42}$$

Equation (20), combined with Eqs. (17), (18) and (40), constitutes a complete dispersion relation of cyclotron maser instability in a dielectric waveguide.

Previous study[1] indicates that the maximum growth rate occurs at the sum of wave admittance $b_-+b_+\approx 0$ characterized by the vacuum TE mode dispersion relation [Eq. (22)] in the region $0\leq r<R_w$. Making use of the definitions $\xi=p_1R_w$, $\eta=p_2R_w$ and $\zeta=p_2R_c$, we can express the vacuum TE mode dispersion relation on Eq. (22) as

$$\omega^2/c^2-k^2=x_{on}^2/R_w^2=\xi^2/R_w^2=(\xi\zeta/\eta)^2/R_c^2 \ , \tag{43}$$

where the parameter ξ is related to η by

$$Z=J_1(\xi)/\xi J_o(\xi)=\frac{J_1(\eta)N_1(\zeta)-J_1(\zeta)N_1(\eta)}{\eta[J_o(\eta)N_1(\zeta)-J_1(\zeta)N_o(\eta)]} \ , \tag{44}$$

for a specified value of parameter ζ. It is instructive to examine Eq. (43) in the limit $\varepsilon\to 1$. Making use of $\xi=\eta$, and Eq. (44), we have $(\omega^2/c^2-k^2)R_c^2=\alpha_{on}^2$ from Eq. (43) for $\varepsilon=1$.

Figure 7 is plots of the impedance Z versus parameter ξ (broken lines) and Z versus parameter η (solid lines) obtained from Eq. (44) for $\zeta=4$, 5 and 6. The scales in horizontal line in Fig. 7 represent both the parameters ξ and η. The solid curves are plotted only for the ranges η satisfying Eq. (42). Note that for specified values of ξ and ζ, the parameter η is determined from Fig. 7. For example, for $\xi=2$, we find from Fig. 7

that η=2.175 for ζ=4, η=3.3 for ζ=5 and η=4.35 for ζ=6 corresponding to the wave impedance Z=1.25 at surface of a dielectric material. In this particular example (ξ=2), values of parameters ξ/η and R_w/R_c are given by (ξ/η, R_w/R_c)=(3.68, 0.54) for ζ=4, (3.03, 0.66) for ζ=5 and (2.70, 0.73) for ζ=6. From the definitions of ξ, η and ζ, we obtain $\omega^2(\varepsilon-1)=c^2(1-\xi^2/\eta^2)\zeta^2/R_c^2$ which unmistakably indicates that the eigenfrequency of vacuum waveguide mode depends on the dielectric constant ε. However, the maximum growth rate of cyclotron maser instability of electron beams characterized by $\beta_z^2<<1$ occurs at the eigenfrequency ω satisfying $\omega^2>>k^2c^2$, thereby approximating $\eta^2/\xi^2=p_2^2/p_1^2$ by

$$\varepsilon=\eta^2/\xi^2 \quad . \tag{45}$$

In this regard, we can approximately determine the dielectric constant ε from Fig. 7 and Eq. (45) for the cyclotron maser instability. As an example, for ξ=2, we obtain ε=1.19 for ζ=4, ε=2.62 for ζ=5, and ε=4.75 for ζ=6. We also emphasize that the impedance Z on Eq. (40) is purely reactive [i.e., Z_i=0 where Z_i is defined in Eq. (25)] for the eigenfrequency ω satisfying $\omega^2>k^2c^2$.

In order to complete the stability analysis of cyclotron maser instability on a dielectric loaded waveguide, it is required to investigate numerically the dispersion relation in Eq. (20), where no a priori assumption is made that the beam is very tenuous. However, use is made of the fact that the magnitude of Doppler-shifted eigenfrequency $|\omega-k\beta_z c-\omega_c|$ is much less than the electron cyclotron frequency (i.e., $|\omega-k\beta_z c-\omega_c|<<\omega_c$). Evaluating the parameters ξ, η, ζ, and the wave admittance b_-+b_+ at $\omega=\omega_o=k\beta_z c+\omega_c$, the dispersion relation in Eq. (20) can be approximated by

$$\left[\omega_c \frac{d}{d\omega}(b_-+b_+)\right]_{\omega_o}\chi^3+(b_-+b_+)_{\omega_o}\chi^2+\frac{\nu}{2\hat{\gamma}}\frac{\beta_\perp^2}{\xi_o^2}\left(\frac{R_w}{R_o}\right)^2\left[\left(1+\beta_z kc/\omega_c\right)^2-(kc/\omega_c)^2\right] \quad =0 \tag{46}$$

where $\Delta_o=(\omega-\omega_o)$, and the normalized Doppler-shifted eigenfrequency χ is defined in Eq. (33). The normalized growth rate $\chi_i=\mathrm{Im}\chi$ has been calculated numerically from Eq. (46) for a broad range of system parameters kc/ω_c, $R_w\omega_c/c$, $R_c\omega_c/c$ and dielectric constant ε. In this numerical calculation, it has been assumed that the beam parameters are $\nu=0.002$, $\hat{\gamma}=1.118$ and $\beta_\perp=0.4$. To maximize the growth rate of instability, we also assumed[3] $R_o\omega_c/c=\alpha_{11}$, where α_{11} is the first root of $J_1'(\alpha_{11})=0$.

Fig. 8 illustrates influence of the self-dielectric effects of an electron beam on the cyclotron maser instability. Shown in Fig. 8 are plots of normalized growth rate χ_i versus kc/ω_c obtained from Eq. (34) (broken line) for $x_{on}=\alpha_{01}$ and $x_{on}R_o/R_w=\alpha_{11}$, and from Eq. (46) (solid line) for $\varepsilon=1$, $R_w\omega_c/c=R_c\omega_c/c=\alpha_{01}/\gamma_z=3.75$. Obviously from Fig. 8, the growth rate calculated from the self-consistent dispersion relation in Eq. (46), including the self-dielectric effects of beam itself, is slightly greater than the growth rate from the approximate dispersion relation in Eq. (34). However, for a low density beam with small transverse velocity ($\beta_\perp^2<<1$) as shown in Fig. 8, self-dielectric effects of beam itself is insignificant.

Stability boundaries in the parameter space ($R_c\omega_c/c$, ε) are illustrated in Fig. 9 for several values of $R_w\omega_c/c$ ranging from 2.2 to 2.8. In Fig. 9, the solid curves correspond to the stability boundaries obtained from Eq. (46) for $\hat{\gamma}=1.118$, $\beta_\perp=0.4$. For a given value of $R_w\omega_c/c$, the region of ($R_c\omega_c/c$, ε) parameter space <u>below</u> the curve corresponds to absolute stability for any arbitrary values of normalized axial wavenumber kc/ω_c, whereas the region of paremeter space <u>above</u> the curve corresponds to instability for some values of wavenumber kc/ω_c. Several points are noteworthy from Fig. 9. First, for general values of the parameter $R_w\omega_c/c$, the stability boundaries converge to the common value $R_c\omega_c/c\simeq 3.6$ for $\varepsilon=1$

corresponding to vacuum dielectric constant. In fact, the stability properties of Eq. (46) are the same for any arbitrary values of $R_w\omega_c/c$ for $\varepsilon=1$. Second, for a given radius of dielectric material, the value of dielectric constant ε required for instability increases rapidly to infinity as the radius of conducting wall ($R_c\omega_c/c$) approaches to the inner radius of dielectric material ($R_w\omega_c/c$). Third, obviously for a given radius of conducting wall, instability occurs even at small values of dielectric constant as the value of parameter $R_w\omega_c/c$ is decreased.

The dependence of stability properties on dielectric constant ε is further illustrated in Fig. 10, where the normalized growth rate χ_i is plotted versus ε for $R_c\omega_c/c=3.75$, $R_w\omega_c/c=2.4$, $kc/\omega_c=0.2$, $\gamma=1.118$, $\beta_\perp=0.4$ and $\nu=0.002$. In these particular parameters, the maximum growth rate $\chi_i=0.024$ occurs at the dielectric constant $\varepsilon=1$. The range of ε corresponding to instability occurs repeatedly as the value of dielectric constant ε is increased to infinity. For example, in Fig. 10, the system is unstable for the dielectric constant ε satisfying $1\leq\varepsilon<2.9$ (first radial harmonic number n=1) and $10.2<\varepsilon<13.2$ (second radial harmonic number n=2). In this value of conducting radius ($R_c\omega_c/c=3.75$), without a dielectric material the system can be unstable only for first radial harmonic number n=1. Since a dielectric material reduces significantly the radial wavelength of the waveguide mode, it is possible to have high radial mode perturbations for a large dielectric constant.

Examining carefully on the cubic equation (46) and noting $(1+kc\beta_z/\omega_c)^2 > (kc/\omega_c)^2$ in a typical cyclotron maser instability, we conclude from Eq. (46) that for instability, $(b_-+b_+)_{\omega_o}>0$, or $|(b_-+b_+)_{\omega_o}|<<1$ for $(b_-+b_+)_{\omega_o}<0$. Moreover, in order to have a smooth unstable spectrum with a broad bandwidth, it is required for the ratio a to satisfy

$$|a| = \left| \frac{b_- + b_+}{\omega_c \frac{d}{d\omega} (b_- + b_+)} \right|_{\omega_o} \ll 0.1 \ , \tag{47}$$

for a considerable range of k space when the beam is very tenuous ($\nu \ll 0.01$).

For present purposes, to illustrate the influence of dielectric material on instability bandwidth, we present in Fig. 11 plots of (a) $(b_- + b_+)_{\omega_o}$, (b) the ratio a and (c) the normalized growth rate χ_i versus kc/ω_c obtained from Eqs. (17), (18), (40) and (46) for $R_w\omega_c/c = 2.4$, $\gamma = 1.118$, $\beta_\perp = 0.4$, $\nu = 0.002$ and several pairs of parameters $(R_c\omega_c/c, \varepsilon)$. Several important features are noteworthy in Fig. 11. First, the matched geometric configuration $(R_c\omega_c/c, \varepsilon) = (3.75, 1)$ is most unstable. However, the range of k space corresponding to instability is narrow. Second, a slightly unmatched configuration $(R_c\omega_c/c, \varepsilon) = (3.75, 2)$ is unstable for a broad range of k space, with a considerably reduced growth rate. Unfavorably, the growth rate for $(R_c\omega_c/c, \varepsilon) = (3.75, 2)$ is a sharply changing function of the wavenumber k. Evidently from Fig. 11(b), the ratio a for $(R_c\omega_c/c, \varepsilon) = (3.75, 2)$ is not satisfying Eq. (47). Third, it is noted from Fig. 11(b) that the ratio a for $(R_c\omega_c/c, \varepsilon) = (3, 6)$ satisfies Eq. (47), thereby resulting in a smooth unstable spectrum with a broad bandwidth on k space. Although the growth rates for this case are slightly reduced from those values of $(R_c\omega_c/c, \varepsilon) = (3.75, 1)$, the range of k space corresponding to instability for this case is almost twice broader than that for $(R_c\omega_c/c, \varepsilon) = (3.75, 1)$. In this regard, the unstable spectrum of $(R_c\omega_c/c, \varepsilon) = (3, 6)$ is most desirable for a communicational application.

We conclude this section by emphasizing that stability properties of cyclotron maser instability in a dielectric loaded waveguide exhibit a sensitive dependence on the dielectric constant ε and thickness of dielectric material. It has been shown that, by an appropriate choice of

ε and thickness of dielectric material, the bandwidth of instability can be increased more than twice of that for a plain conducting waveguide, slightly reducing the growth rate of instability. Moreover, dielectric material reduces the radial wavelength of the waveguide mode, thereby significantly modifying the nature of perturbations.

VI. CONCLUSIONS

In this paper we have investigated the influence of finite wall impedance effects on the cyclotron maser instability of a hollow electron beam in a waveguide with an arbitrary impedance Z. The stability analysis has been carried out within the framework of the linearized Vlasov-Maxwell equations, assuming that the beam thickness is much less than the equilibrium radius R_o of the beam. The formal stability analysis for azimuthally symmetric electromagnetic perturbations ($\partial/\partial\theta=0$) has been carried out in Sec. II, including the influence of finite wall impedance Z. In Sec. III, properties of the vacuum TE mode dispersion relation have been investigated in the absence of a beam. A detailed analytic and numerical investigation of cyclotron maser instability has been carried out in Sec. IV for a wall impedance independent of the eigenfrequency and axial wavenumber. One of the most important features of this analysis is that, for a purely resistive wall, the growth rate is substantially reduced by introducing even a very small amount of resistivity into the wall. Moreover, the range of kc/ω_c corresponding to instability increases rapidly as the resistivity of wall is increased. Cyclotron maser stability properties in a dielectric loaded waveguide have been investigated in Sec. V. It has been shown that stability properties of cyclotron maser instability exhibit a sensitive dependence on the dielectric constant ε and thickness of dielectric material. By an appropriate choice of ε and thickness of dielectric material, the bandwidth of instability can be increased more than twice of that for a plain conducting waveguide.

ACKNOWLEDGMENTS

This research was supported by the Independent Research Fund at the Naval Surface Weapons Center.

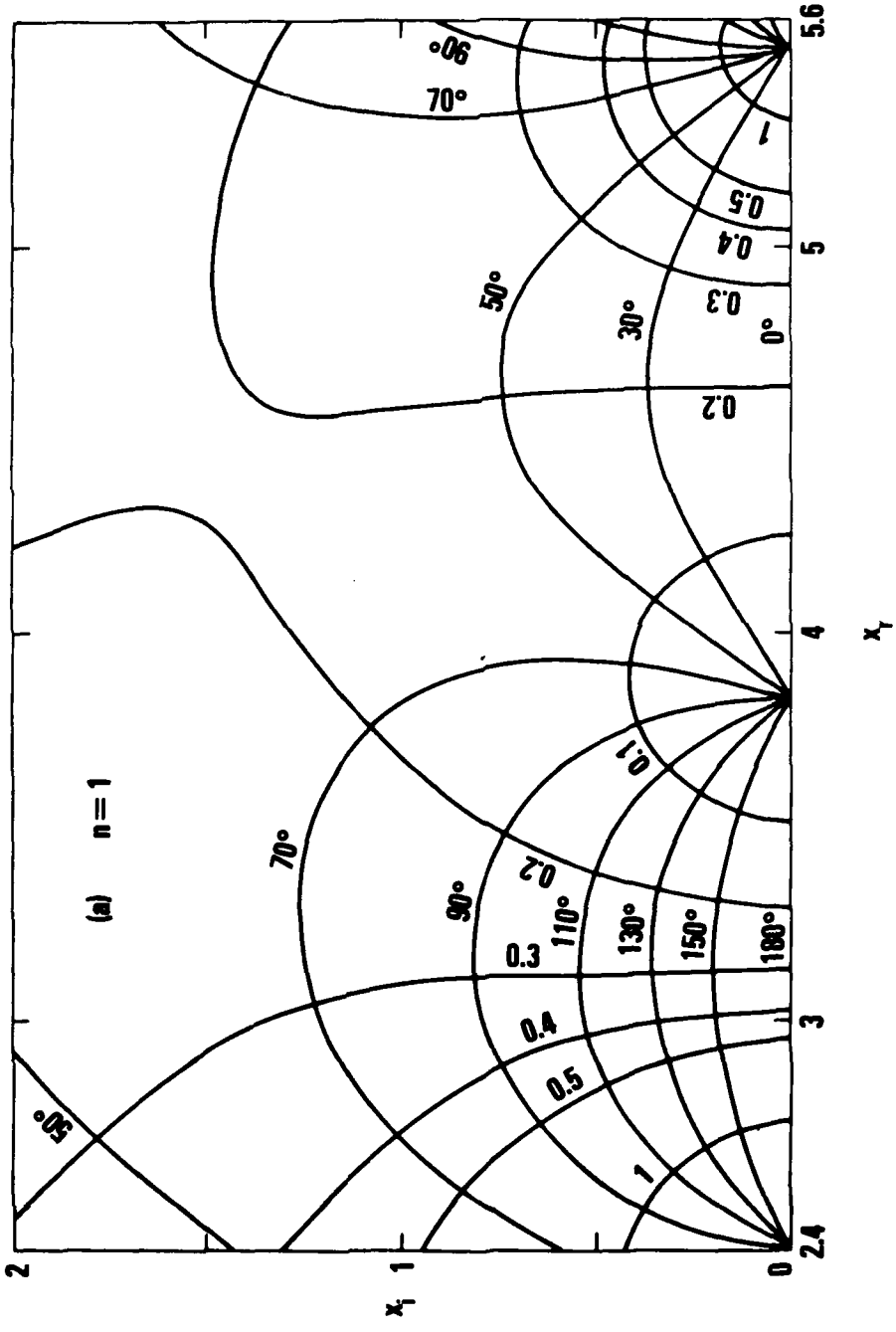

Figure 1a - Contours of Constant Phase Angle ϕ and Magnitude $|Z|$ of Function $Z=J_1(x_{on})/x_{on}J_1(x_{on})$ in the Plane of the Root $x_{on}=x_r-x_i$ for n=1.

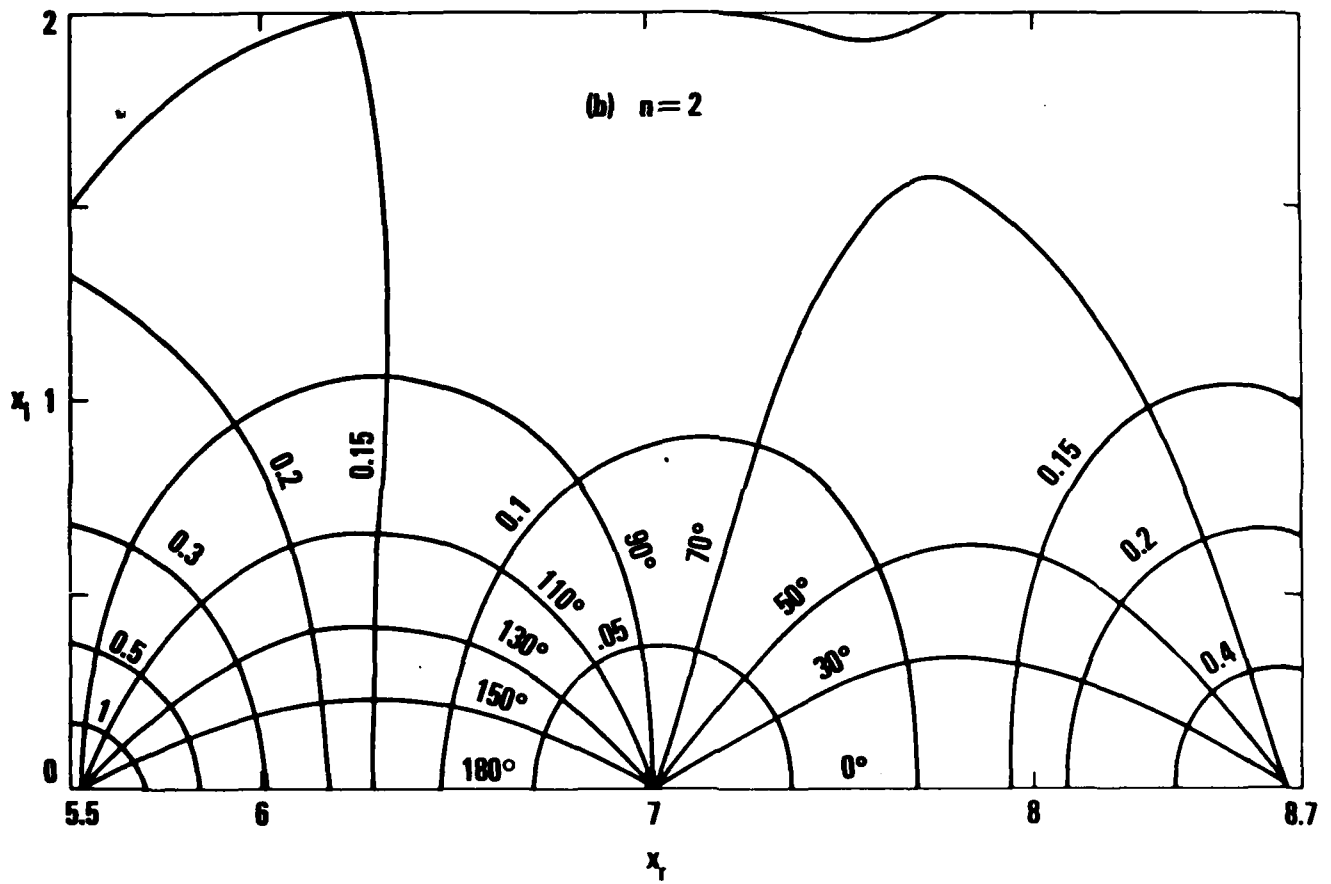

Figure 1b - Contours of Constant Phase Angle ϕ and Magnitude $|Z|$ of Function $Z=J_1(x_{on})/x_{on}J_1(x_{on})$ in the Plane of the Root $x_{on}=x_r-x_i$ for n=2.

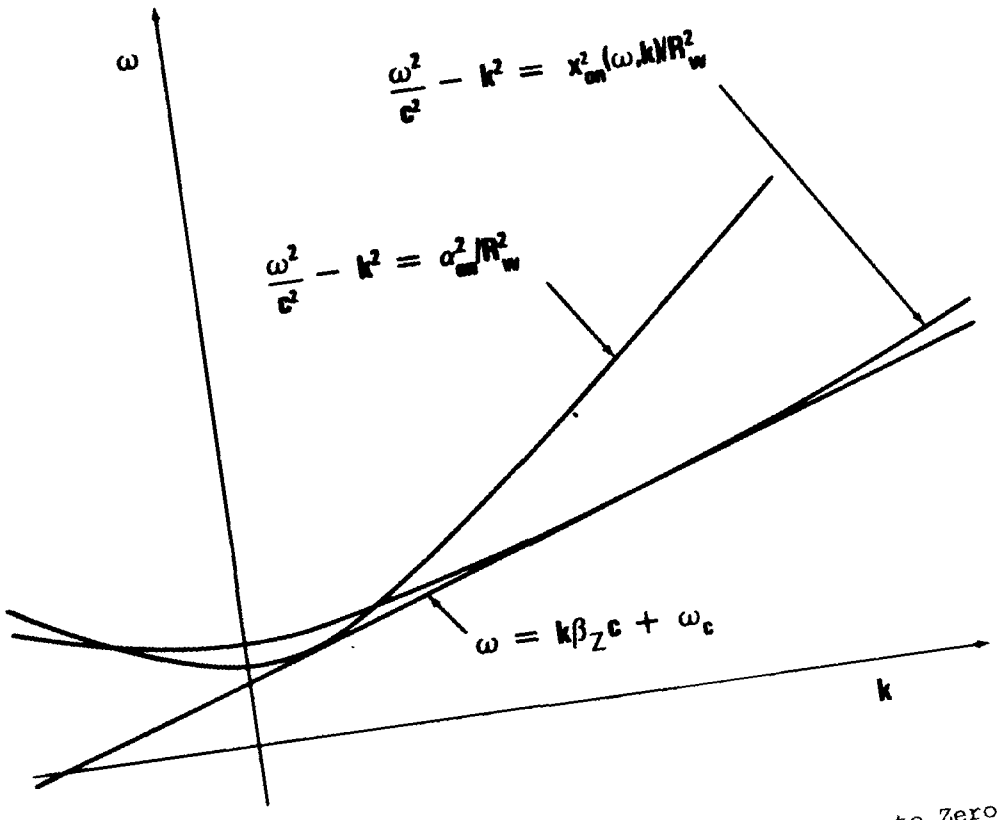

Figure 2 - Schematic Drawings of the Curve $\omega=(k^2c^2+\alpha_{on}^2c^2/R_w^2)^{1/2}$ Corresponding to Zero Wall Impedance and the Curve $\omega=(k^2c^2+x_{on}^2c^2/R_w^2)^{1/2}$ Corresponding to an Arbitrary Wall Impedance Z. The straight line $\omega=k\beta_z c+\omega_c$ is the Cyclotron Resonance Mode.

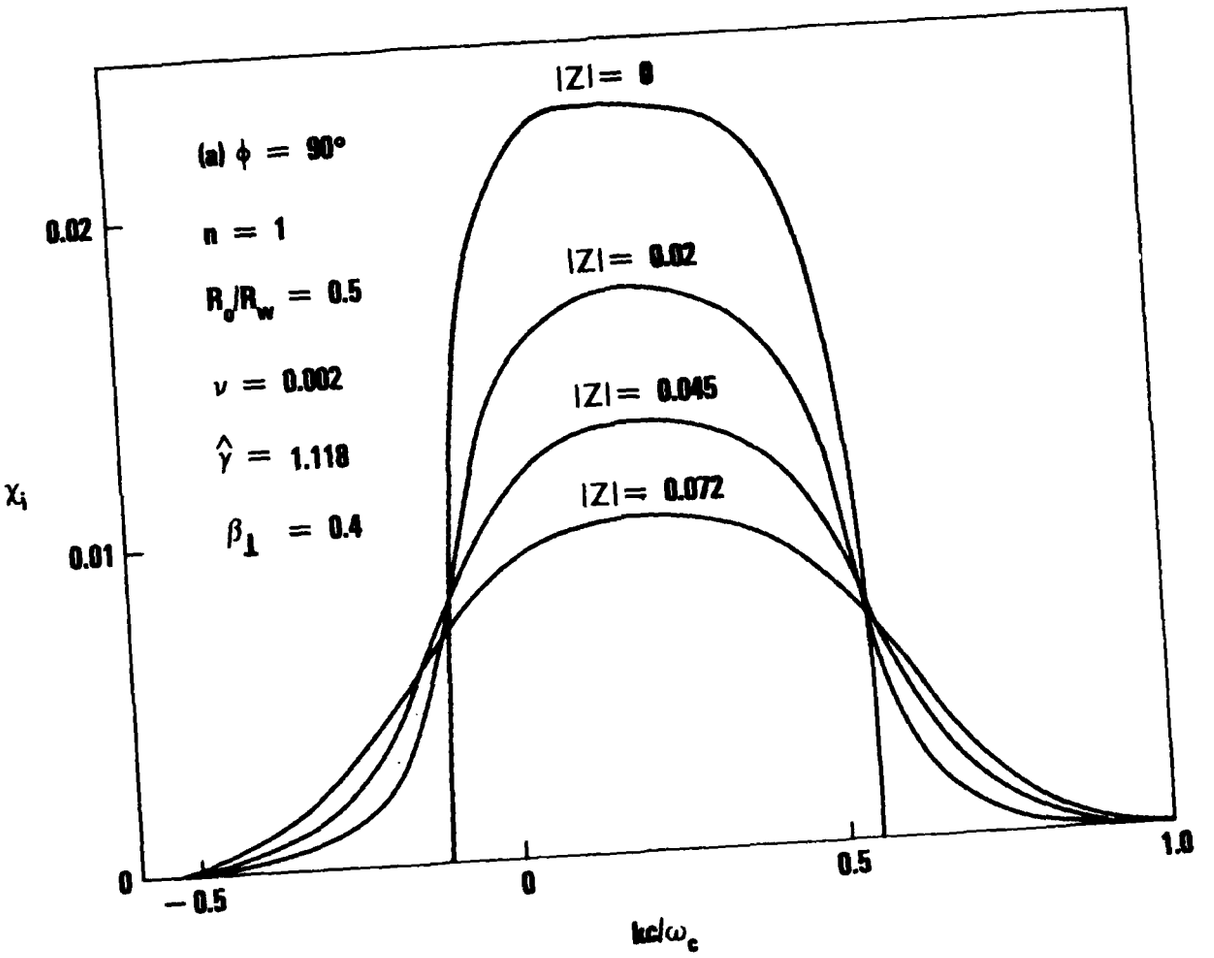

Figure 3a - Plots of the Normalized Growth Rate χ_i.

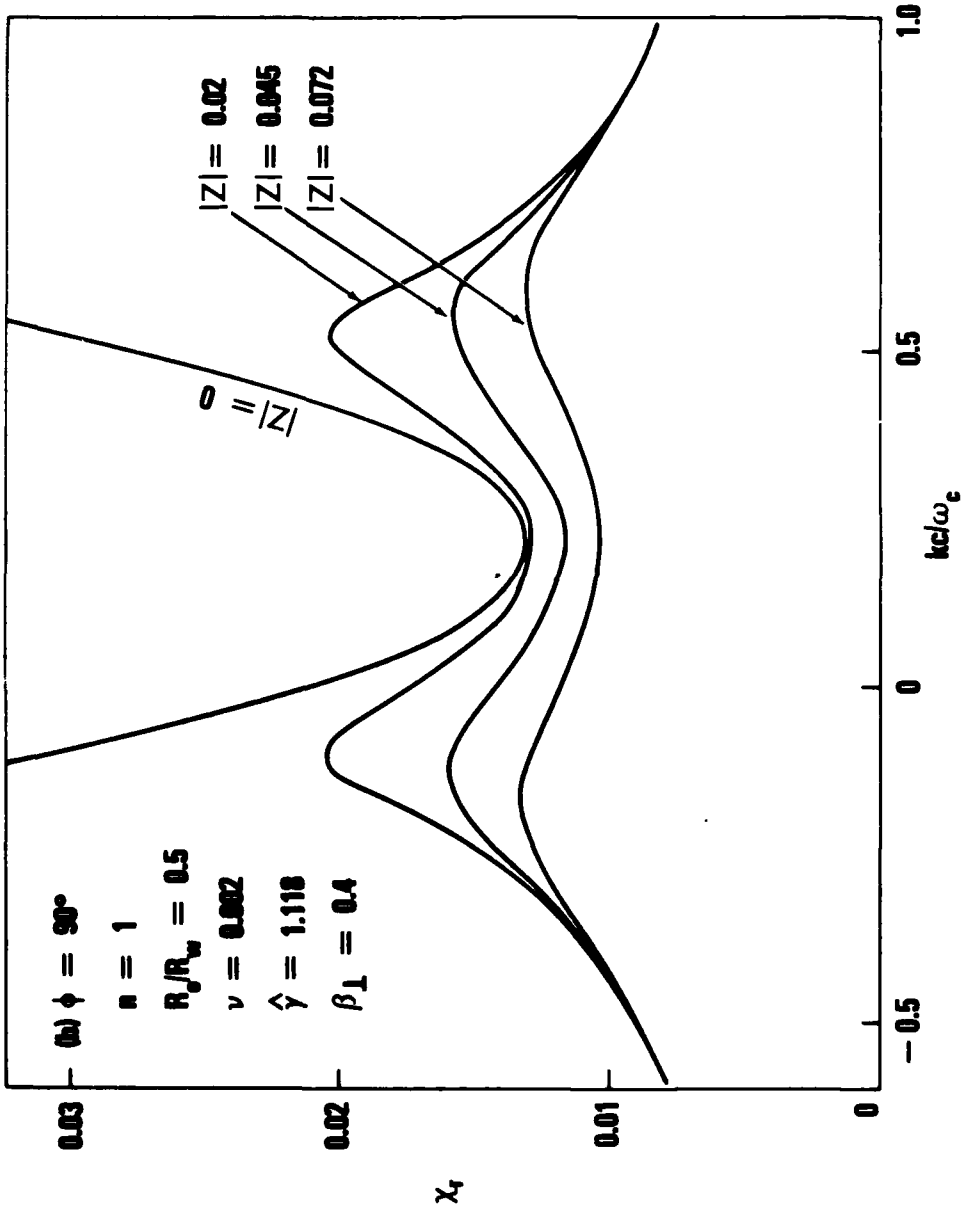

Figure 3b - Plots of the Normalized Doppler-Shifted Real Frequency χ_r Versus kc/ω_c [Eq. (34)] for ν=0.002, $\hat{\gamma}$=1.118, $\beta_\perp$=0.4, n=1, R_o/R_w=0.5, ϕ=90°, and Several Values of |Z|.

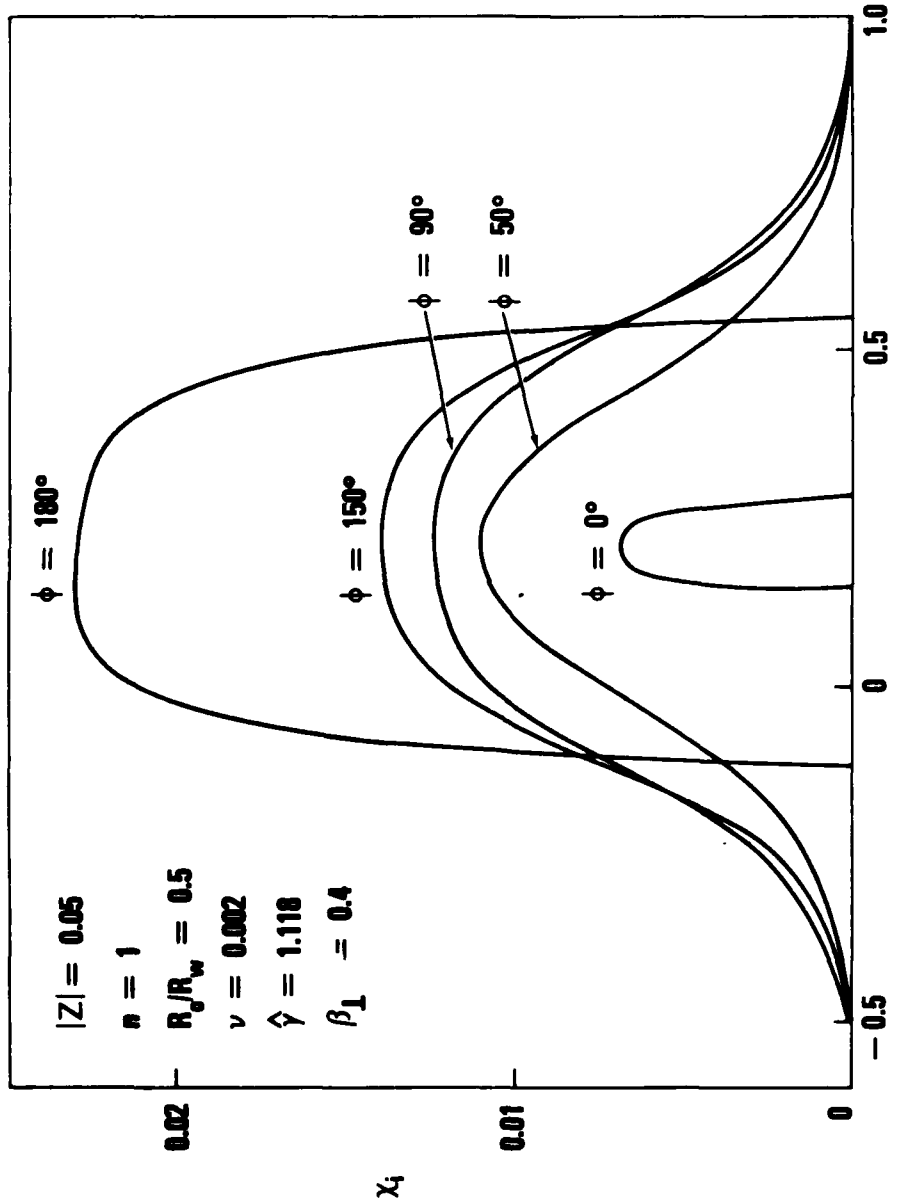

Figure 4 - Plots of the Normalized Growth Rate χ_i Versus kc/ω_c for $|Z|=0.05$, Several Different Phase Angles ϕ, and Parameters Otherwise Identical to Fig. 3.

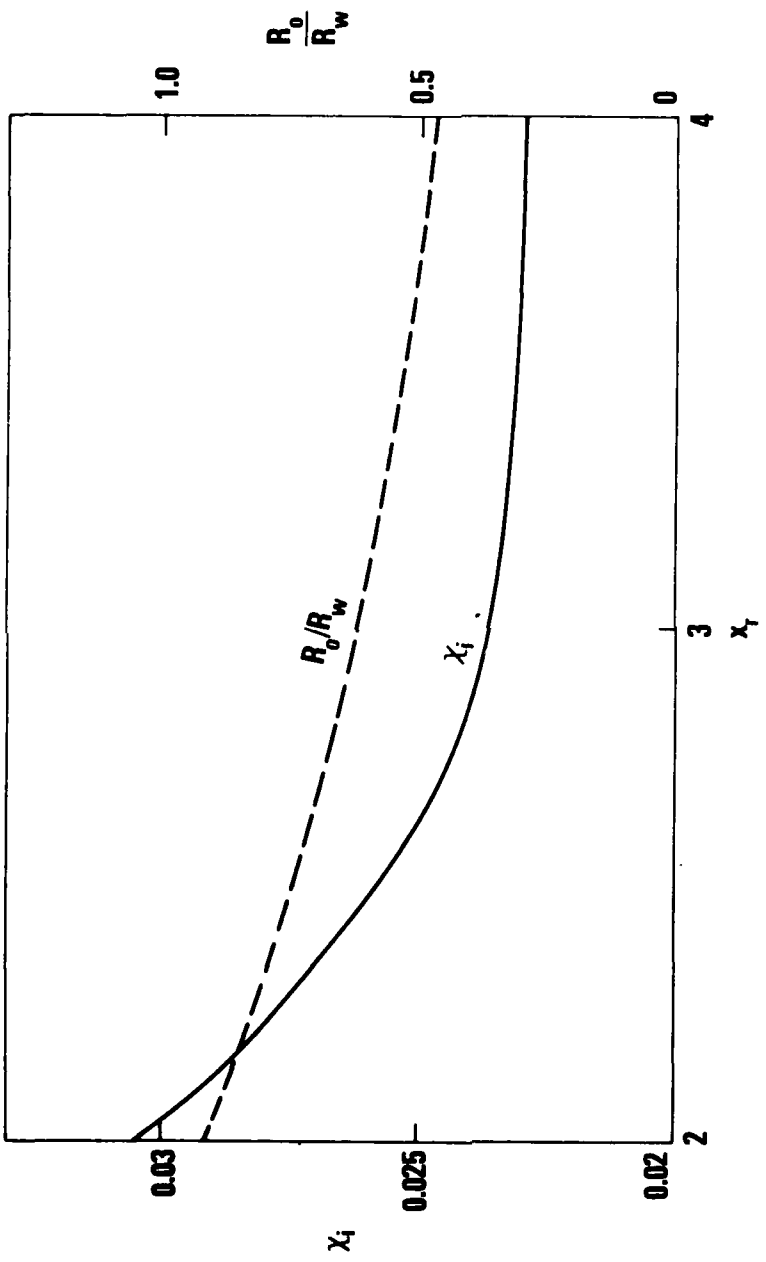

Figure 5. Plots of Normalized Maximum Growth Rate (Solid Line) and $R_o/R_w = \sqrt{11}/x_{on}$ (Broken Line) Versus $x_{on}=x_r$ [EQS. (36) and (35)] for the Parameters Identical to Fig. 3.

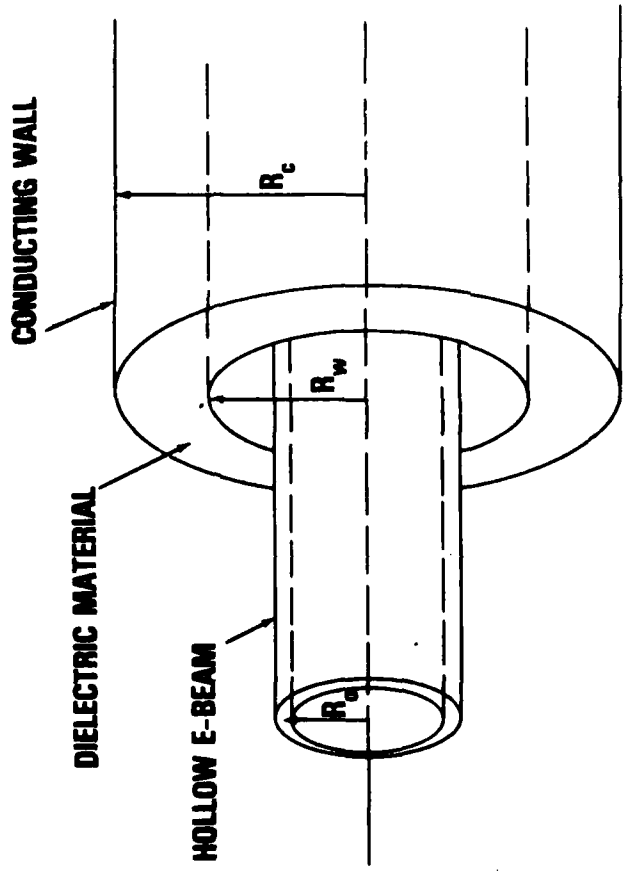

Figure 6 - Equilibrium Configuration of a Hollow Electron Beam on a Dielectric Loaded Waveguide.

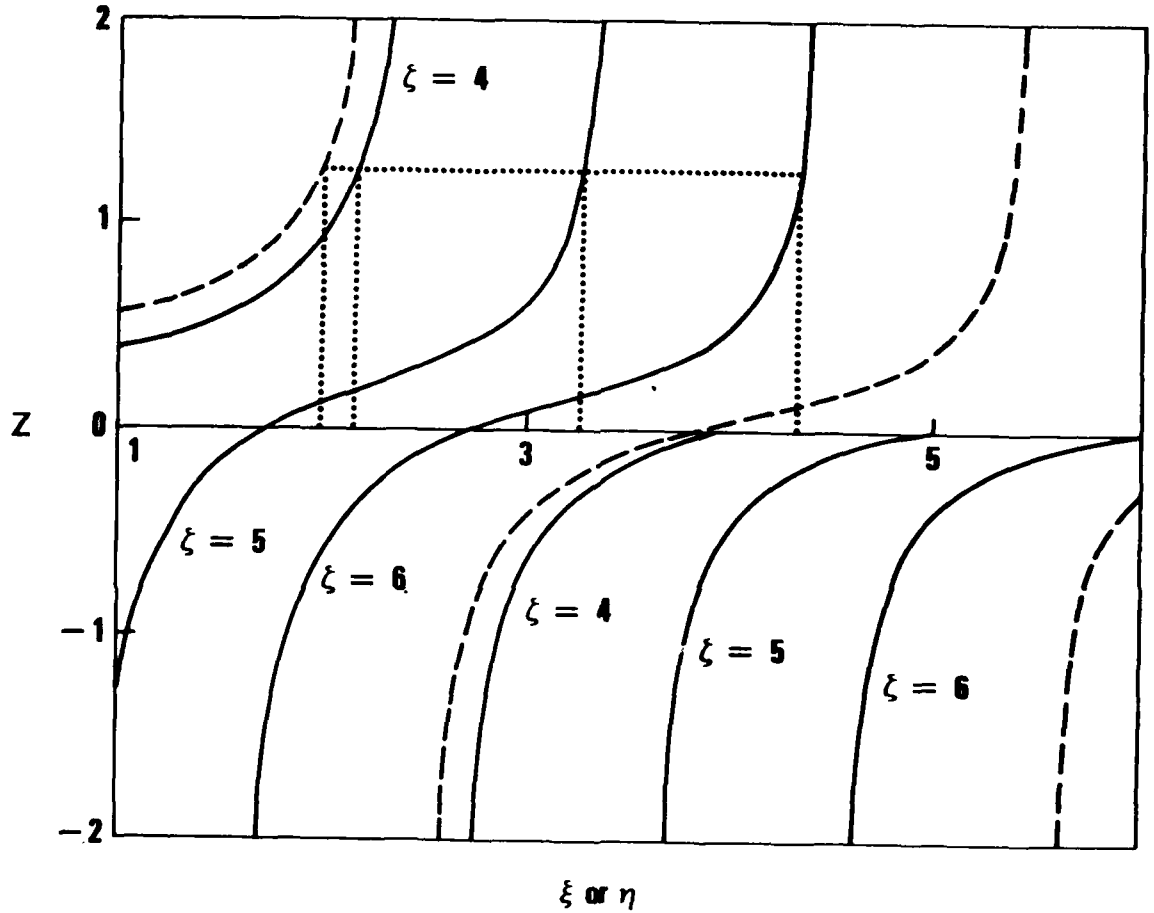

Figure 7 - Plots of Impedance Z Versus Parameter ξ (Broken Line) and Z Versus Parameter η (Solid Lines) [Eq. (44)] for ζ=4, 5, and 6. Scales in Horizontal Line represent Both the Parameters ξ and η.

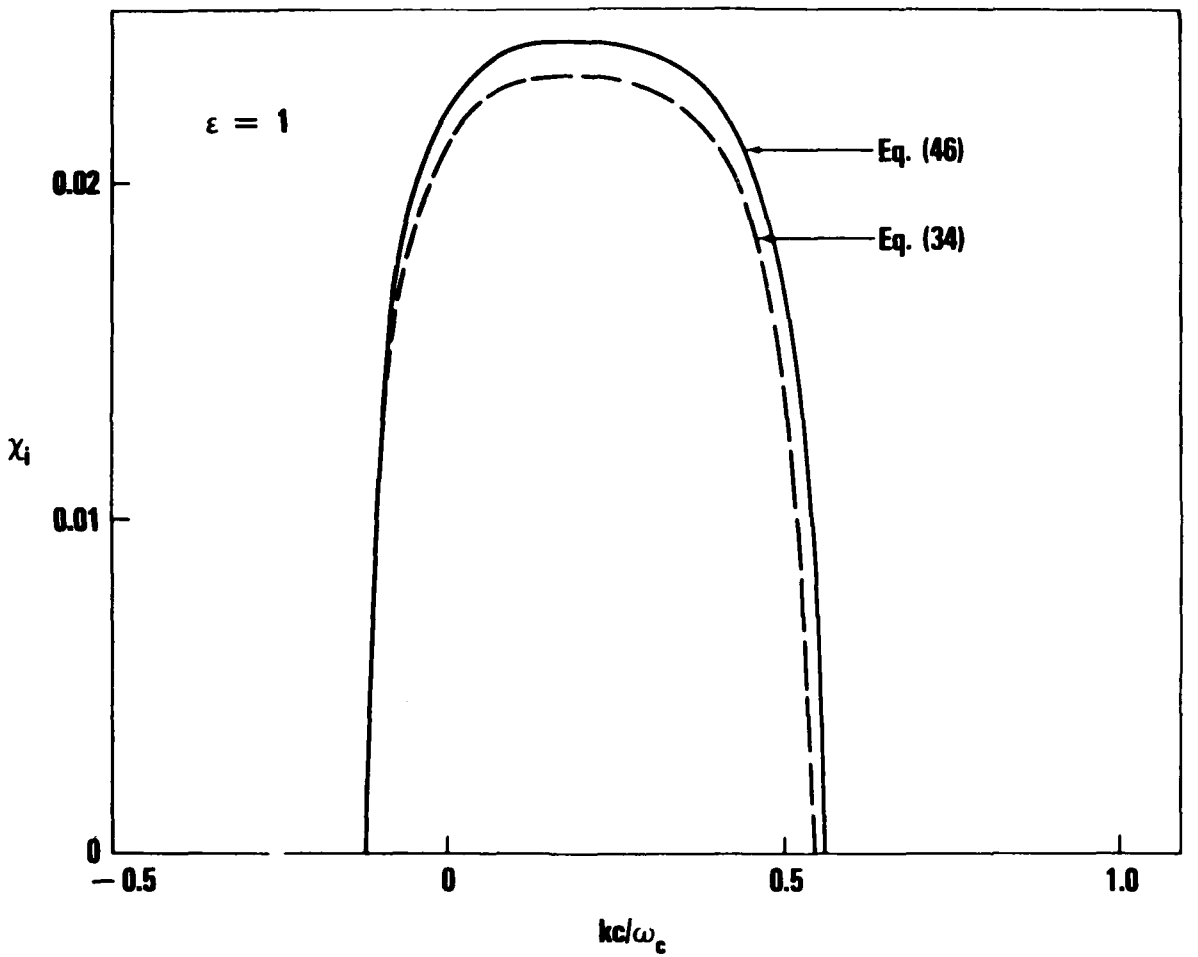

Figure 8 - Plots of the Normalized Growth Rate χ_i Versus kc/ω_c Obtained from the Approximate Dispersion Relation in EQ. (34) (Broken Line) for $x_{on}=\alpha_{on}$ and $x_{on}R_o/R_w=\alpha_{11}$, and from the Self-Consistent Dispersion Relation in EQ. (46) (Solid Line) for $\varepsilon=1$, $R_w\omega_c/c=R_c\omega_c/c=3.75$.

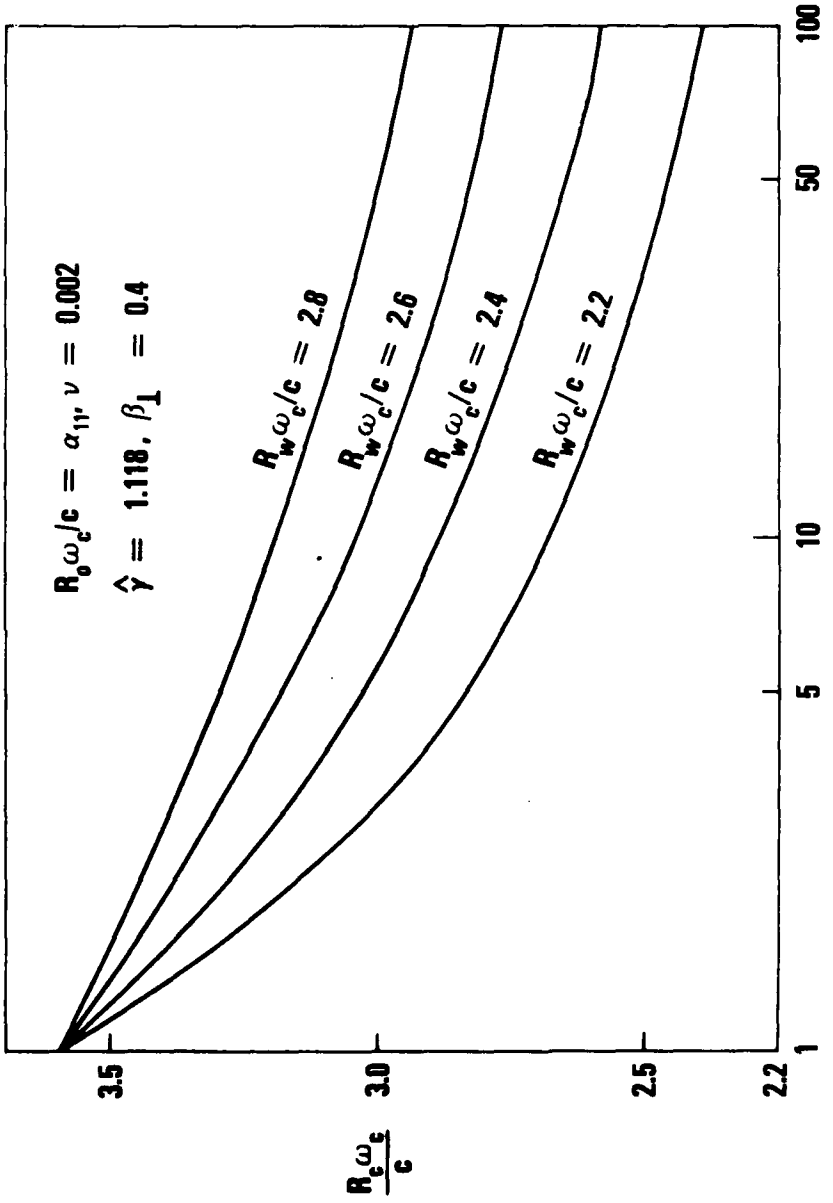

Figure 9 - Stability Boundaries [EQ. (46)] in the Parameter Space (R_{c_c}/c,) for $R_{o_c}/c=\alpha_{11}$, Several Values of $R_w\omega_c/c$ and Parameters Otherwise Identical to Fig. 3.

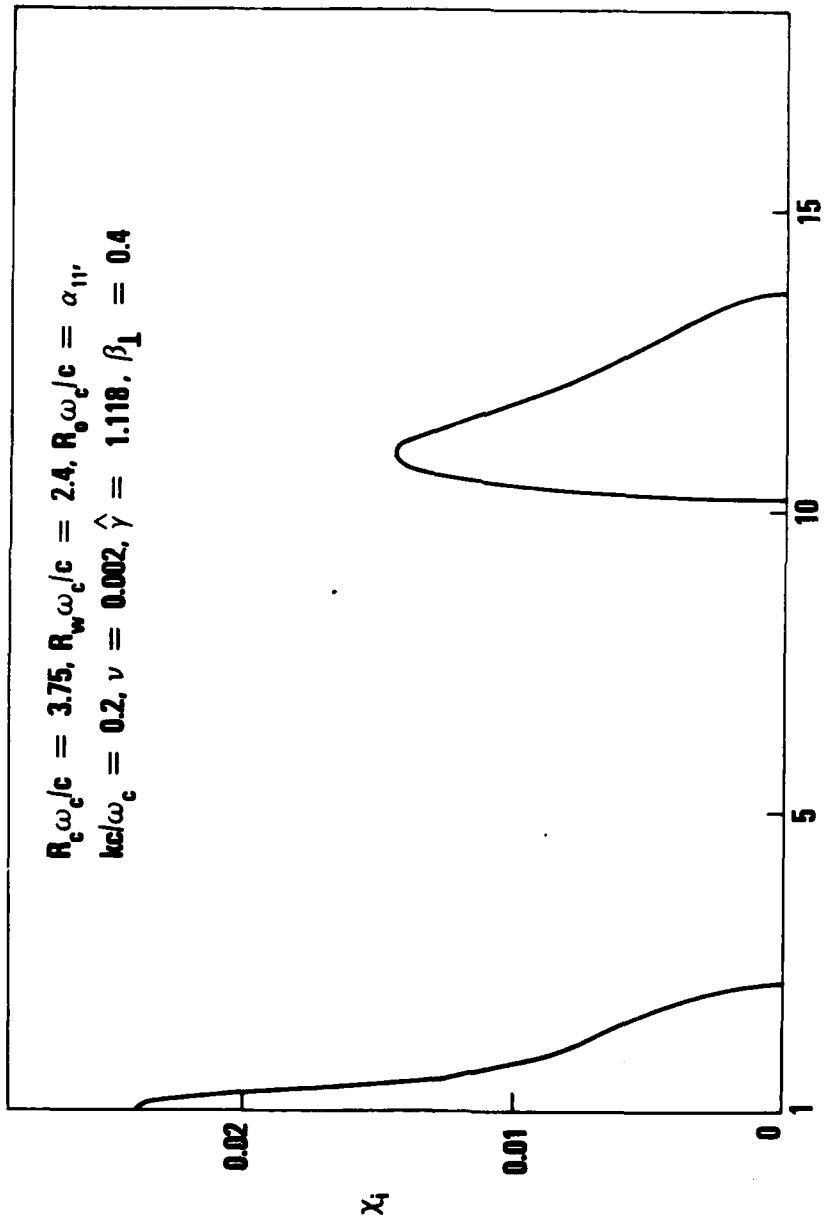

Figure 10 - Plots of the Normalized Growth Rate χ_i Versus ε [EQ. (46)] for $R_c\omega_c/c=3.75$, $R_w\omega_c/c=2.4$, $R_o\omega_c/c=\alpha_{11'}$, $kc/\omega_c=0.2$, and Parameters Otherwise Identical to Fig. 3.

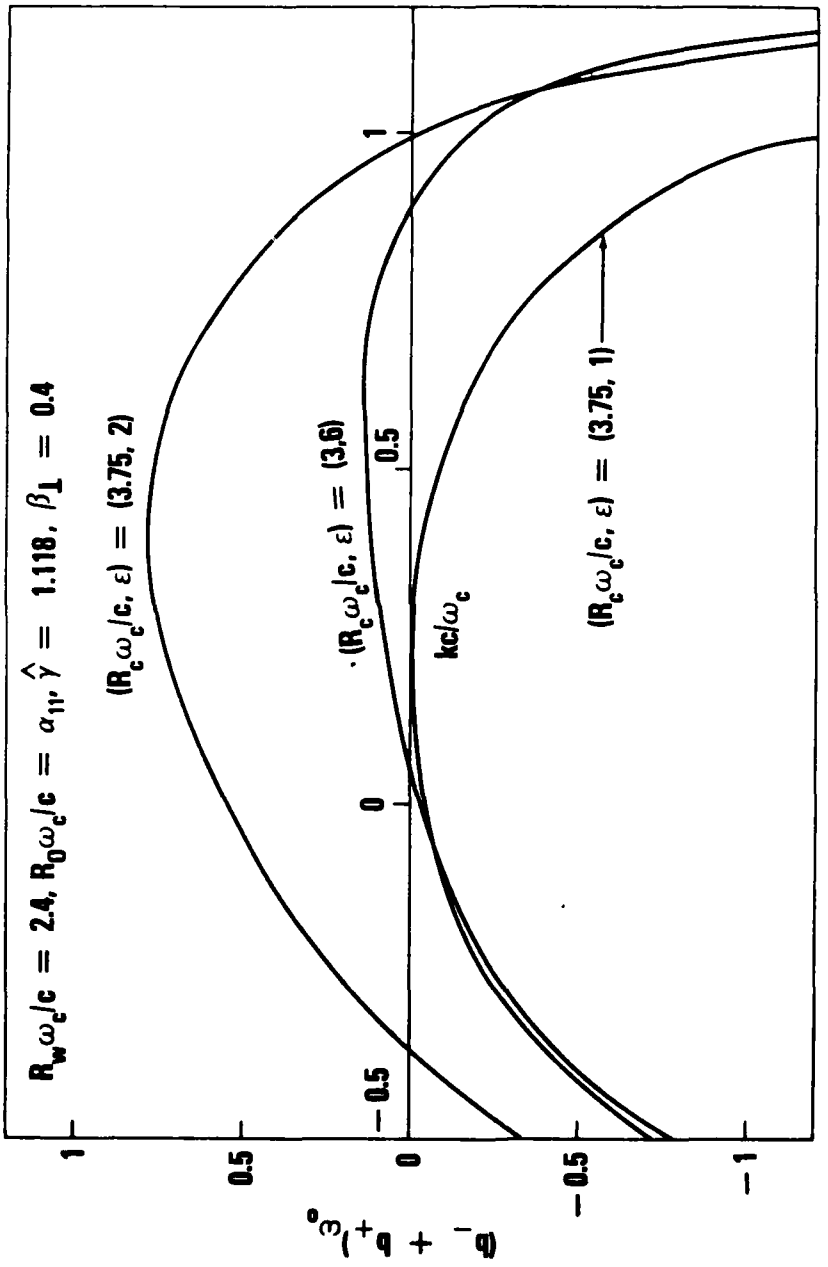

Figure 11a - Plots of $(b_- + b_+)/\omega_o$.

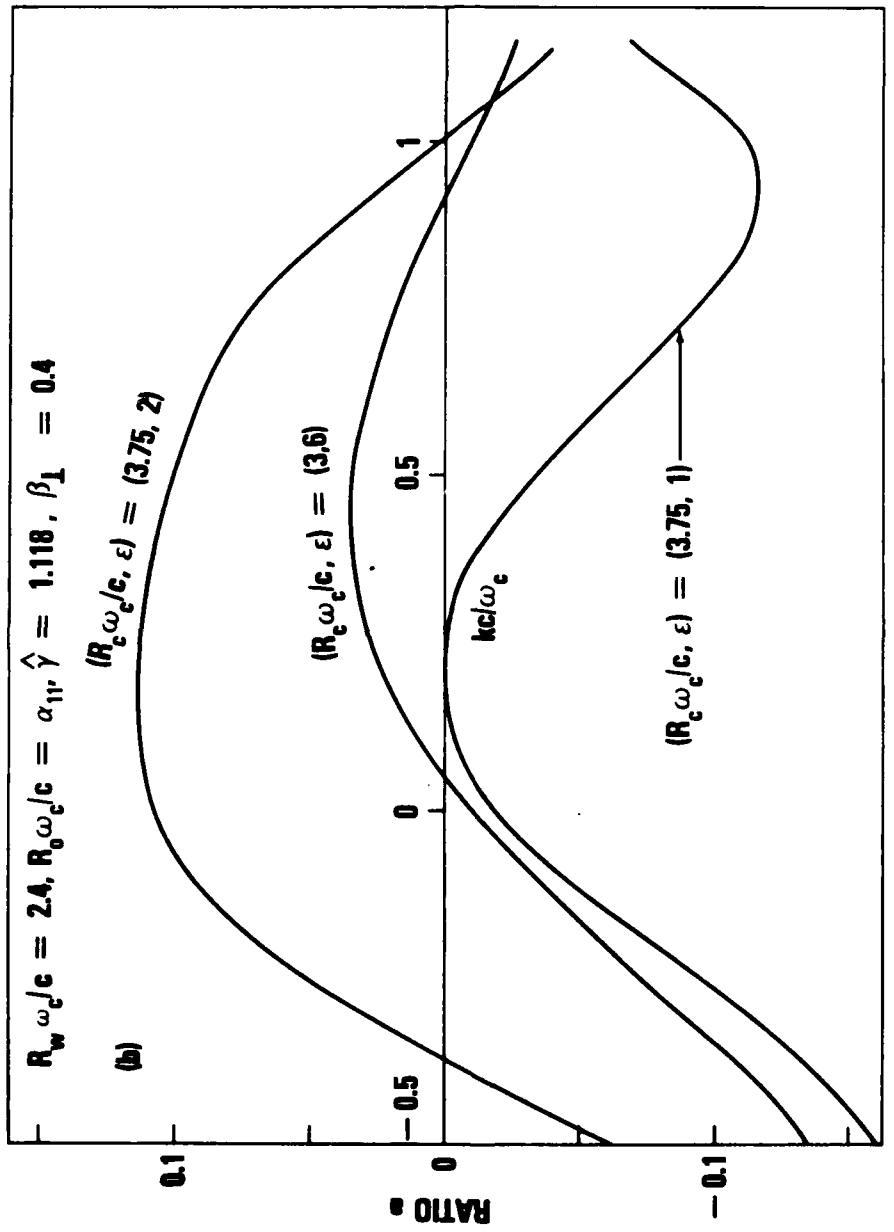

Figure 11b - Plots of the Ratio a.

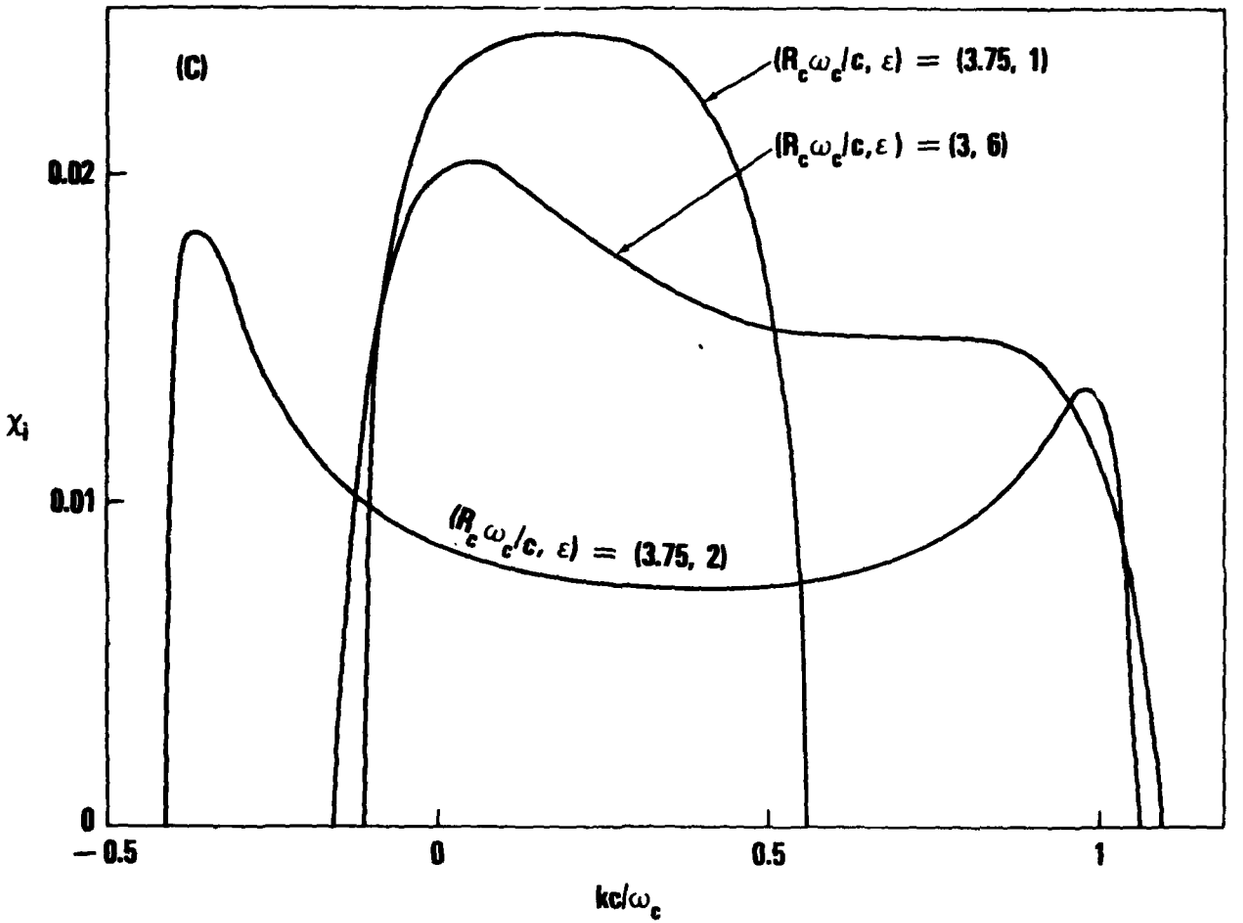

Figure 11c - Plots of the Normalized Growth Rate χ_i Versus kc/ω_c [EQS. (17), (18), (40) and (46)] for $R_w\omega_c/c=2.4$, Several Pairs of Parameters $(R_c\omega_c,\varepsilon)$ and Parameters Otherwise Identical to Fig. 3.

REFERENCES

1. H. S. Uhm, R. C. Davidson, and K. R. Chu, Phys. Fluids 21, 1866 (1978).

2. V. A. Flyagin, A. V. Gaponov, M. I. Petelin, and V. K. Yulpatov, IEEE Trans. Microwave Theory Tech. MTT-25, 514 (1977).

3. H. S. Uhm, R. C. Davidson, and K. R. Chu, Phys. Fluids 21, 1877 (1978).

4. P. Sprangle and A. T. Drobot, IEEE Trans. Microwave Theory Tech. MTT-25, 528 (1977).

5. H. S. Uhm and R. C. Davidson, Phys. Fluids 22, 1804 (1979).

6. K. R. Chu, Phys. Fluids 21, 2354 (1978).

7. H. S. Uhm and R. C. Davidson, Phys. Fluids 22, 1811 (1979).

8. E. Ott and W. M. Manheimer, IEEE Trans. Plasma Sci. PS-3, 1 (1975).

9. H. S. Uhm and R. C. Davidson, J. Appl. Phys. 50, 696 (1979).

10. J. L. Hirshfield, I. B. Bernstein, and J. M. Wachtel, IEEE J. Quantum Electron. QE-1, 237 (1965).

11. V. L. Granatstein, P. Sprangle, R. K. Parker, M. Herndon, and S. P. Schlesinger, J. Appl. Phys. 46, 3800 (1975).

12. N. I. Zaytsov, T. B. Pankratova, M. I. Petelin, and V. A. Flyagin, Radio Eng. Electron. Phys. 19, 103 (1974).

13. M. Friedman, D. A. Hammer, W. M. Manheimer, and P. Sprangle, Phys. Rev. Lett. 31, 753 (1973).

14. J. R. Pierce, Traveling-Wave Tubes, (D. Van Nostrand Company, Inc., New York, 1950) Chap. 4.

15. C. K. Birdsall and J. P. Whinnery, J. Appl. Phys. 24, 314 (1953).

DISTRIBUTION

	Copies
Naval Research Laboratory Attn: Dr. M. Lampe Dr. J. Siambis Washington, D.C. 20365	 1 1
Office of Naval Research Attn: W.J. Condell (ONR-421) Washington, D.C. 20350	2
U.S. Army Ballistic Research Laboratory Aberdeen Proving Ground Attn: Dr. D. Eccleshall (DRDAR-BLB) Aberdeen, Maryland 21005	1
Air Force Weapons Laboratory Kirtland Air Force Base Attn: Maj. H. Dogliani Albuquerque, New Mexico 87117	1
Department of Energy Attn: Dr. T. Godlove (C-404) Washington, D.C. 20545	1
National Bureau of Standards Attn: Dr. J.M. Leiss Gaithersburg, Maryland 20760	1
Austin Research Associates, Inc. Attn: Dr. W.E. Drummond 1901 Rutland Drive Austin, Texas 78758	1
Ballistic Missile Defense Advanced Technology Center Attn: Dr. L.J. Harvard (BMDSATC-1) P.O. Box 1500 Huntsville, Alabama 35807	1
B-K Dynamics, Inc. Attn: Dr. R. Linz 15825 Shady Grove Road Rockville, Maryland 20850	1

DISTRIBUTION (cont)

	Copies
The Charles Stark Draper Laboratory, Inc. Attn: Dr. E. Olsson 555 Technology Square Cambridge, Massachusetts 02139	1
Director Defense Advance Research Projects Agency Attn: Dr. J. Mangano 1400 Wilson Boulevard Arlington, Virginia 22209	1
IRT Corporation Attn: Mr. W. Selph P.O. Box 81087 San Diego, California 92138	1
Los Alamos Scientific Laboratory Attn: Dr. G. Best P.O. Box 1663 Los Alamos, New Mexico 87545	1
Mission Research Corporation Attn: Dr. C. Longmire 735 State Street Santa Barbara, California 93102	1
Physical Dynamics, Inc. Attn: Dr. K. Breuckner P.O. Box 977 La Jolla, California 92037	1
Sandia Laboratories Attn: Mail Services Section for: Dr. R.B. Miller Albuquerque, New Mexico 87115	1
Science Applications, Inc. Attn: Dr. M.P. Fricke 1200 Prospect Street La Jolla, California 92037	1

DISTRIBUTION (cont)

	Copies
Science Applications, Inc. Attn: Dr. R. Johnston 2680 Hanover Street Palo Alto, California 94304	1
University of California Lawrence Livermore Laboratory Attn: Dr. R.J. Briggs Dr. E. Lee P.O. Box 808 Livermore, California 94550	1 1
Defense Technical Information Center Cameron Station Alexandria, Virginia 22314	12
Naval Sea Systems Command Washington, D. C. 20362 Attn: SEA-09G32 SEA-03B	2 1

NDW-NSWC(W)-5605/1 (Rev. 5-78)

TO AID IN UPDATING THE DISTRIBUTION LIST FOR NAVAL SURFACE WEAPONS CENTER, WHITE OAK TECHNICAL REPORTS PLEASE COMPLETE THE FORM BELOW:

TO ALL HOLDERS OF NSWC/TR 80-131
by Han S. Uhm, Code R41

DO NOT RETURN THIS FORM IF ALL INFORMATION IS CURRENT

A. FACILITY NAME AND ADDRESS *(OLD) (Show Zip Code)*

NEW ADDRESS *(Show Zip Code)*

B. ATTENTION LINE ADDRESSES:

C.

☐ REMOVE THIS FACILITY FROM THE DISTRIBUTION LIST FOR TECHNICAL REPORTS ON THIS SUBJECT.

D.

NUMBER OF COPIES DESIRED _____

END

DATE
FILMED

8-80

DTIC